ELSEVIER

Chemical Geology 202 (2003) 155–182

CHEMICAL GEOLOGY
INCLUDING
ISOTOPE GEOSCIENCE

www.elsevier.com/locate/chemgeo

Iron isotope fractionation during oceanic crust alteration

Olivier Rouxel[a,*], Nicolas Dobbek[a], John Ludden[a], Yves Fouquet[b]

[a] *CRPG-CNRS, 15 Rue Notre Dame des Pauvres, 54500 Vandoeuvre, France*
[b] *IFREMER DRO/GM, BP 70, 29280 Plouzané, France*

Accepted 4 August 2003

Abstract

The purpose of this work is to study the mobility and budget of Fe isotopes in the oceanic crust and in particular during low-temperature interaction of seawater with oceanic basalt. We carried out this investigation using samples from Ocean Drilling Program (ODP) Site 801C drilled during Leg 129 and Leg 185 in Jurassic Pacific oceanic crust seaward of the Mariana Trench. The site comprises approximately 450 m of sediment overlying a section of 500 m of basalt, which includes intercalated pelagic and chemical sediments in the upper basaltic units and two low-temperature (10–30 °C) ocherous Si–Fe hydrothermal deposits. Fe was chemically separated from 70 selected samples, and $^{57}Fe/^{54}Fe$ ratios were measured by MC-ICP-MS Isoprobe. The isotopic ratios were measured relative to an internal standard solution and are reported relative to the international Fe-standard IRMM-14. Based on duplicate measurements of natural samples, an external precision of 0.2 ‰ (2σ) has been obtained. The results indicate that the deep-sea sediment section has a restricted range of $\delta^{57}Fe$, which is close to the igneous rock value. In contrast, large variations are observed in the basaltic section with positive $\delta^{57}Fe$ values (up to 2.05 ‰) for highly altered basalts and negative values (down to −2.49 ‰) for the associated alteration products and hydrothermal deposits. Secondary Fe-minerals, such as Fe-oxyhydroxides or Fe-bearing clays (celadonite and saponite), have highly variable $\delta^{57}Fe$ values that have been interpreted as resulting from the partial oxidation of Fe^{2+} leached during basalt alteration and precipitated as Fe^{3+}-rich minerals. In contrast, altered basalts at Site 801C, which are depleted in Fe (up to 80%), display an increase in $\delta^{57}Fe$ values relative to fresh values, which suggest a preferential leaching of light iron during alteration. The apparent fractionation factor between dissolved Fe^{2+} and Fe remaining in the mineral is from 0.5 ‰ to 1.3 ‰ and may be consistent with a kinetic isotope fractionation where light Fe is stripped from the minerals. Alternatively, the formation of secondary clays minerals, such as celadonite during basalt alteration may incorporate preferentially the heavy Fe isotopes, resulting in the loss of light Fe isotopes in the fluids.

Because microbial processes within the oceanic crust are of potential importance in controlling rates of chemical reactions, Fe redox state and Fe-isotope fractionation, we evaluated the possible effect of this deep biosphere on Fe-isotope signatures. The Fe-isotope systematics presented in this study suggest that, even though iron behavior during seafloor weathering may be mediated by microbes, such as iron-oxidizers, $\delta^{57}Fe$ variations of more than 4 ‰ may also be explained by abiotic processes. Further laboratory experiments are now required to distinguish between various processes of Fe-isotope fractionation during seafloor weathering.

Keywords: Iron isotopes; Oceanic crust; Alteration; Seafloor hydrothermal systems; Deep biosphere

* Corresponding author. Department of Earth Sciences, University of Cambridge, Downing Street, Cambridge CB2 3EQ, UK. Tel.: +44-1223-333405; fax: +44-1223-333450.

E-mail addresses: orou02@esc.cam.ac.uk (O. Rouxel), john.ludden@cnrs-dir.fr (J. Ludden), fouquet@ifremer.fr (Y. Fouquet).

0009-2541/$ - see front matter © 2003 Elsevier B.V. All rights reserved.
doi:10.1016/j.chemgeo.2003.08.011

1. Introduction

Alteration of oceanic crust by seawater is one of the most important processes controlling global fluxes of the elements (Staudigel and Hart, 1983). Low-temperature interaction of seawater with the upper oceanic crust is an important sink for seawater alkalis, Mg, ^{18}O, C and H_2O (Staudigel et al., 1996; Alt and Teagle, 1999; Wheat and Mottl, 2000). The uppermost 400 m of basaltic oceanic crust is characterized by high permeability, and basalts in this zone react with oxygenated deep-sea water to form secondary minerals, including Fe-oxyhydroxides, smectite and celadonite (Alt, 1995; Honnorez, 1981). These phases replace glass, olivine, sulfides and, to lesser extents, plagioclase and clinopyroxene, and they fill fractures and void space in the crust.

Recently, microbes have been shown to play a significant role in the alteration of the oceanic crust (Fisk et al., 1998; Torsvik et al., 1998; Furnes et al., 2001b). The evidence for this deep biosphere includes: alteration textures in volcanic glasses, which are paleotraces of bacterial activity (Fisk et al., 1998); the presence of DNA in altered zones (Furnes et al., 2001a); localized high organic C, N, P and K contents (Torsvik et al., 1998); and the light isotopic composition of C (Furnes et al., 2001a). Iron oxidation (and reduction) and sulfide oxidation are among the potential energy sources for rock-hosted chemoautotrophic microorganisms (Bach and Edwards, in press).

The use of Fe isotopes to trace geochemical and biological cycling of Fe has received a great interest in the past few years (Beard et al., 2003 and references therein). The potential of Fe isotopes for detecting bio-signatures in natural systems has been recently argued by Beard et al. (1999). These proposed bio-signatures are based on relatively constant Fe-isotope ratios in igneous rocks and a significant range in sedimentary settings (Beard et al., 1999). Furthemore, laboratory evidence of microbe-induced Fe-isotope fractionation suggests that dissimilatory reduction of Fe (Beard et al., 1999) and dissolution of Fe-silicates in the presence of catecholate siderophores (Brantley et al., 2001) may produce isotopic variations of up to 1‰ of $^{56}Fe/^{54}Fe$ ratio. Abiotic Fe-isotope fractionation during ion exchange chromatography has been observed by Anbar et al. (2000) and has been proposed to reflect the importance of isotopic fractionation between Fe chloro-aquo complexes. Furthermore, equilibrium and kinetic isotopic fractionation between Fe(III) and Fe(II) complexes may produce a large isotopic shift comparable to or greater than that produced by microbially mediated reduction of ferrihhydrite (Bullen et al., 2001; Johnson et al., 2002; Matthews et al., 2001). Several workers have predicted significant equilibrium Fe-isotope fractionation based on spectroscopic data for various minerals (Polyakov and Mineev, 2000) and aqueous Fe species (Schauble et al., 2001). Although extensive experimental investigation of Fe isotopic fractionation are still needed, these theoretical calculation may be, to a first approximation, suitable for predicting signs of Fe-isotope fractionation between fluids and minerals.

The extensive redox reactions, dissolution and precipitation of Fe-bearing minerals that occur during oceanic crust alteration should result in Fe-isotope fractionation that may be used to trace bio-geochemical processes in such environments. Recent investigation of Fe isotopes in hot spring along the Juan de Fuca Ridge showed that Fe isotopes are fractionated in hydrothermal systems (Sharma et al., 2001). High-temperature alteration of the oceanic crust could therefore provide a source of isotopically light Fe to the deep oceans (Sharma et al., 2001) and thus contribute to Fe isotopic variations observed in deep-sea sediments such as Mn nodules (Zhu et al., 2000a,b). In this study, we present data that define the Fe-isotope signatures of the upper oceanic crust recovered at three Ocean Drilling Program (ODP) Sites (ODP Sites 801, 1149 and 765). These data are used to evaluate the processes that may produce Fe-isotope fractionation during low-temperature alteration of basalts and to document the effect of these process in the geochemical cycle of Fe in oceanic systems. Site 801 is a reference site in the Jurassic oceanic crust and offers a unique opportunity to study the alteration of old oceanic crust and the isotopic budget of Fe isotopes. An important goal of this study was to explore the potential effects of the biological activity associated with the alteration of the oceanic crust on Fe-isotope signatures.

2. Field setting and samples

This investigation involved a collection of sediments, basalts and interflow materials from ODP Sites

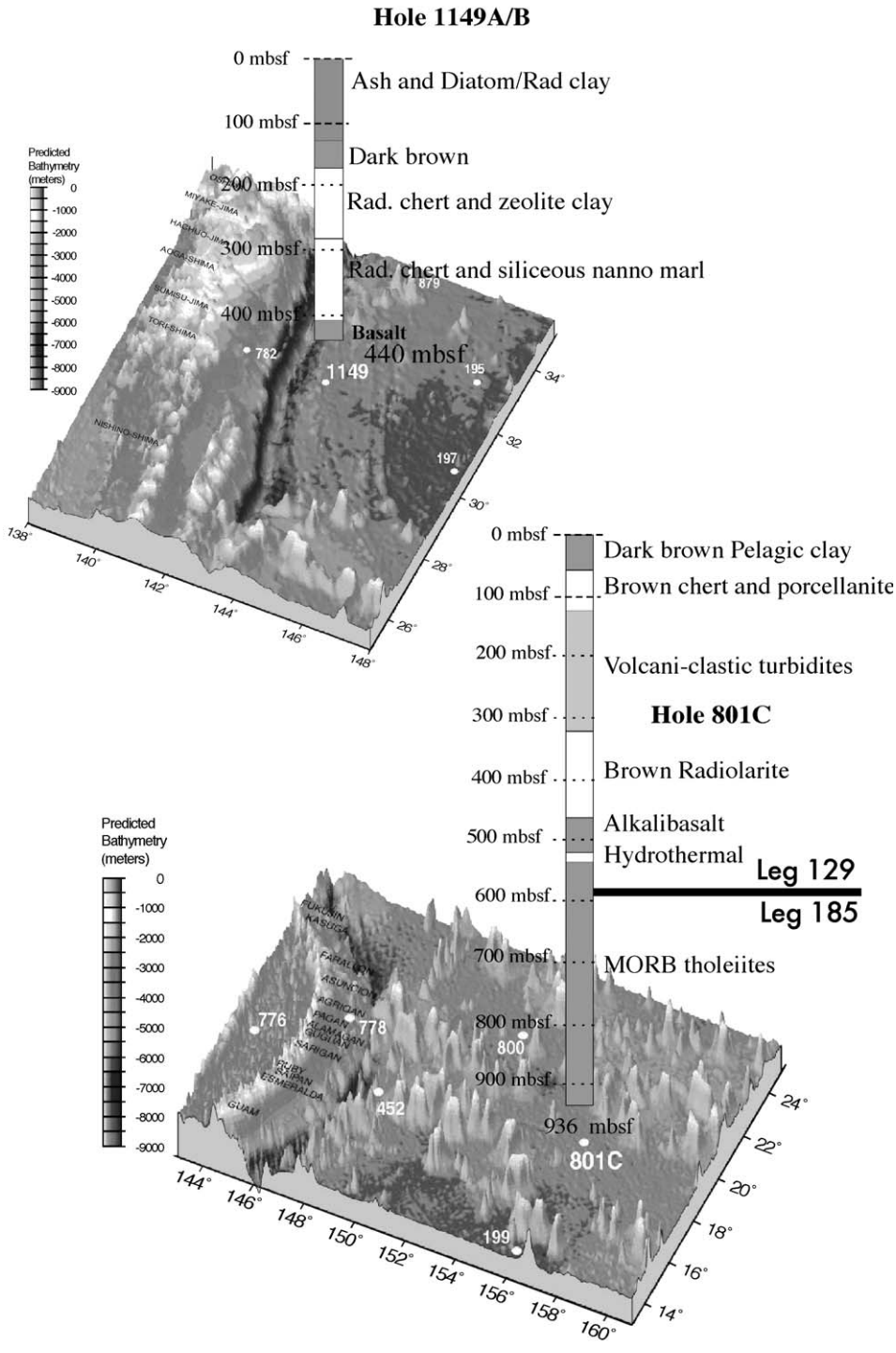

Fig. 1. Perspective map of West Pacific (Izu and Mariana arcs) and location of ODP Hole drilled during Leg 185 (Plank et al., 2000). Simplified stratrigraphic columns of Site 1149 and 801 are shown and described in Plank et al. (2000) and Larson and Lancelot (1992).

801 and 1149 drilled during ODP Leg 129 (Larson and Lancelot, 1992) and Leg 185 (Plank et al., 2000) in Cretaceous and Jurassic Pacific oceanic crust seaward of the Mariana Trench (Fig. 1). Additional samples from Site 765 (Leg 123; Gradstein and Ludden, 1990) in the Argo Abyssal Plain located in the eastern Indian Ocean were also included in this study. The alteration pattern of basement at Site 765 has been described previously by Gillis et al. (1992). More detailed information concerning tectonic setting, sedimentology, basement lithology and drilling operations are presented in Plank et al. (2000).

2.1. Lithology

The basaltic section at Site 801 is overlain by a sedimentary section characterized by an upper (65 m) pelagic clay unit, which overlies a 63-m-thick chert-porcelanite unit (Fig. 1). These sedimentary units are underlain by a thick sequence (192 m) of volcanoclastic turbidites of probable Albian age, which represent redeposited material from the Magellan Seamounts. A second chert-radiolarite unit (125 m) underlies the volcanoclastics and gives way to 20 m of Callovian red rediolarites and claystones. At Site 1149, the sediment/basement boundary was recovered in three holes at 410 mbsf in Hole 1149B, at 401 mbsf in Hole 1149C and at 307 mbsf in Hole 1149D (Fig. 1). Compared to Site 801, the sediment section at Site 1149 lacks the major volcanoclastic sequence and is composed primarily of pelagic clays, cherts and siliceous nannofossil marl (Plank et al., 2000).

On the basis of flow morphology, geochemistry and mineralogy, the basement section at Hole 801C (reached at 461.6 mbsf) has been divided into four major sequences and includes rocks drilled on both Leg 129 and Leg 185. The uppermost basement is composed of alkaline basaltic to dolerite sills. The igneous units are intercalated with chert-rich sediments, which are often baked at the contact with the basalt (Fig. 2a). This alkaline sequence is 60.2 m thick and overlies a Si- and Fe-oxyhydroxide-rich hydrothermal horizon. Below the hydrothermal deposit, the volcanic rocks (MORB Unit I) comprise thin flows and pillows, lying above series of thick lava flows. Between 600 and 720 mbsf, the section is characterized by a pillow-dominated zone with well-developed interpillow horizon (MORB Unit II). The amount of interpillow material of probable chemical and sedimentary origin decreases significantly downsection in this unit. A second Si–Fe-rich hydrothermal unit similar to the thicker one uphole is present within MORB Unit II pillows (Fig. 2b). From 720 mbsf to the bottom at 936 mbsf, the MORB Unit III comprises a tectonic breccia that separates a massive flow unit (720–890 mbsf) and a series of thin, generally <1-m-thick sheet flows and pillows (890–934 mbsf).

The MORB basement at Site 801 is punctuated by discrete zones of alteration between intervals of minimally altered basalts. The alteration pattern is thus in contrast with a simple downhole decreases in the extent of oxidative alteration observed at other sites drilled by ODP (Alt et al., 1986; Staudigel et al., 1996). These discrete zones occur adjacent to ocherous, Fe–Si-rich, low-temperature hydrothermal deposits and near breccias probably related to near-axis faults. Away from these alteration zones, fresh basaltic glass is abundant, demonstrating the heterogeneous distribution of low-temperature seafloor alteration. Volcanic glass recovered throughout the section is altered by invasive channels and tubes (Fisk, 1999) that are similar to other examples in basaltic glass in the deep ocean crust and that have been attributed to microbial alteration (Fisk et al., 1998).

2.2. Alteration patterns

All of the studied rocks have been affected by low-temperature alteration resulting in various combina-

Fig. 2. Photo of major lithologies. (a) Section 185-801C showing extreme alteration types observed. The pale green alteration flanks an interpillow sediment. The gray-green alteration at the bottom of the core is typical of much of the background alteration in the cores. The Fe content of pale green altered basalt may be depleted by as much as 80% compared to gray-green less altered basalts. (b) The top of the core is composed of Si–Fe ochreous hydrothermal deposits. These rocks contain abundant Fe-oxyhydroxides filaments, which have been attributed to be produced by Fe-oxidizing bacteria (Alt et al., 1992). (c) Typical dark green alteration halos and associated gray diabase at Site 1149 and similar to those observed at Site 765. Typical basalt consists of internal kernels of dusky red with some light brown-gray mottling. These are surrounded by dark halos (green) and a brown-orange halo adjacent to the vein. (1) Dark green halo composed of celadonitic phyllosilicates. (2) Veins composed of goethite and smectite. (3) Dusky red core regions with light brown mottling.

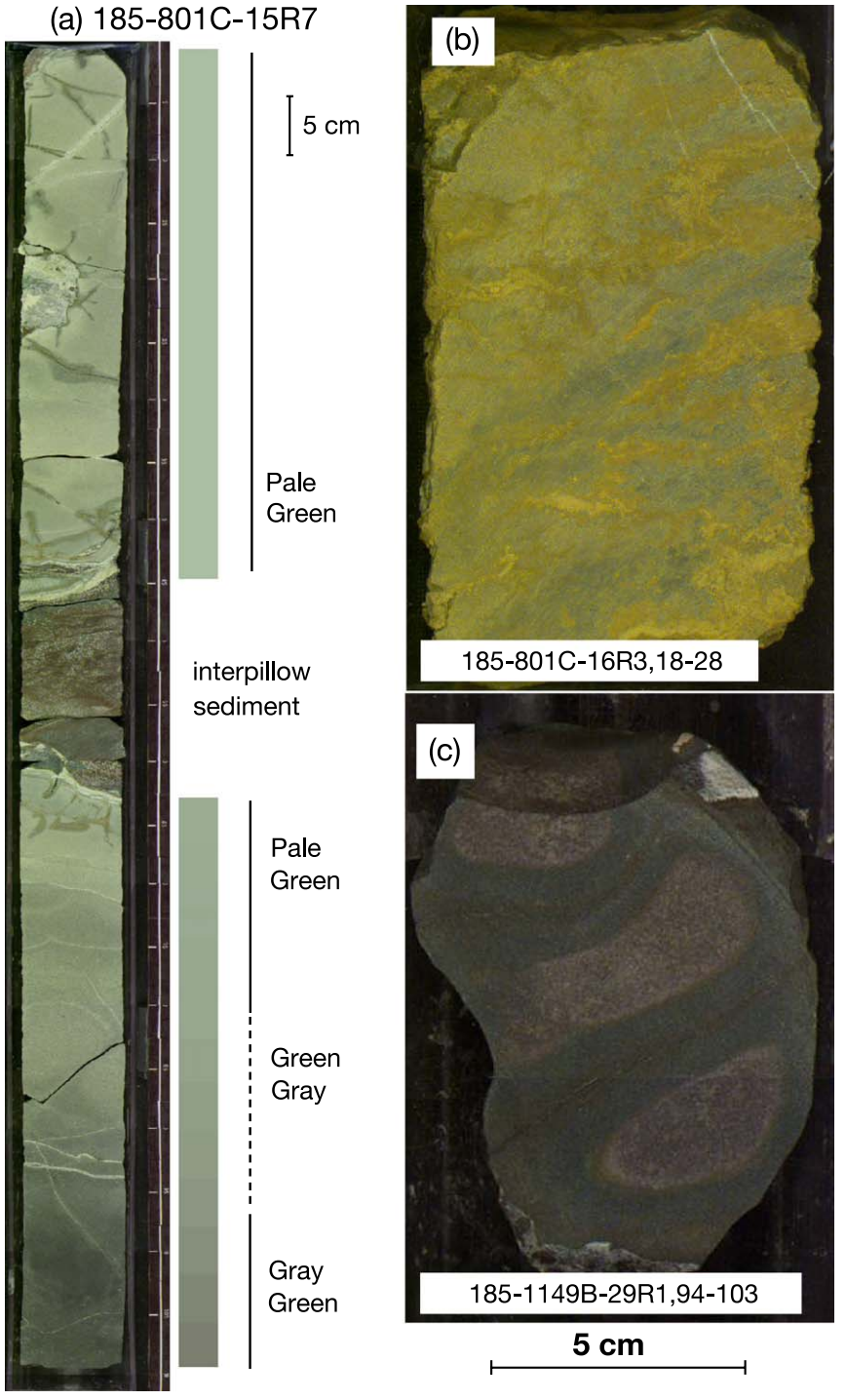
(a) 185-801C-15R7
5 cm
Pale
Green
interpillow
sediment
Pale
Green
Green
Gray
Gray
Green
(b)
185-801C-16R3,18-28
(c)
185-1149B-29R1,94-103
5 cm

tions of secondary minerals both as replacements of igneous phases and as vesicules and cracks fillings. Among the most marked features of the low-temperature alteration of the rocks studied is a pervasive pale green "sage" to gray-green color at Site 801 (Fig. 2a), which contrasts with a concentric color zonations from dusky red to dark or black halos surrounding inner gray core at Sites 1149 and 765 (Fig. 2c).

At Site 801, the two hydrothermal deposits control the distribution of alteration of the underlying basalts. Both are underlain by variably oxidized zones and include zones of buff-colored basalt that have been extensively oxidized (Fig. 2). The most extreme alteration is in the tholeiitic basalts below the hydrothermal zones (MORB Unit I and II). These rocks are characterized by pervasive alteration of the igneous material to bleached pale green rocks, with plagioclase, olivine and pyroxene variably replaced by smectite, celadonite and calcite (Alt et al., 1992). Chemical changes are also the greatest for these rocks, with large increases in alkalis, oxidation and hydration and losses of Ca, Na, Fe and Mg (Alt et al., 1992). The hydrothermal deposit (Fig. 2b) consists of spherules, aggregates and filaments of Fe-oxhydroxide cemented by quartz. It is interpreted to be a low-temperature Fe-oxide deposit, similar to those actively forming on the seafloor at temperature <30 °C, which has later been silicified (Alt et al., 1992). Although similar Fe–Si-rich, low-temperature hydrothermal deposits have been described near modern mid-ocean ridges (Alt, 1988; Boyd and Scott, 2001; Juniper et al., 1992), they have never been cored in other sections of oceanic basement. Thread-like filaments of orange Fe-oxyhydroxide are locally present in the deposits at Site 801 and are remarkably similar to those produced by Fe-oxidizing bacteria (Alt et al., 1992).

Altered basalts recovered at Sites 1149 and 765 are characterized by nonpervasive, oxidative alteration, typical of seafloor weathering (Gillis et al., 1992; Plank et al., 2000). The rocks are variably altered to an assemblage of celadonite, Fe-oxyhydroxides, calcite and saponite and are composed of well-developed alteration halos that are parallel to fracture surfaces and extend several centimeters into the surrounding rock (Fig. 2c). During this alteration stage, volcanic glass, the most readily altered phase, and sulfide, olivine and Ti-magnetite supplied Fe to the alteration fluids allowing the precipitation of Fe-rich minerals such as celadonite and Fe-oxyhydroxides, thus forming the oxidation front at the contact of the halo with the inner gray zone (Talbi and Honnorez, 2003).

2.3. Samples

The samples selected for this study cover the major lithologies recovered at ODP Site 801C. These are deep-sea clays, cherts, interflow sediments, hyaloclastites, Si–Fe-rich hydrothermal deposits, variably altered basalts and alteration products in veins. Vein materials, such as mixed celadonite and Fe-oxhydroxide assemblage, and pyrite veins have been separated by hand-picking from crushed specimens. Diabase and alteration halos have been separated by precise sawing. Solid sample surfaces were cleaned with a sand-blaster and washed in distilled water. Sample powders were prepared using agate grinding vessels.

In addition, we analyzed composite samples. These are physical mixtures of a subset of individual samples representative of different lithologies recovered at Site 801C. The procedures adopted for the preparation of the composites are described in Plank et al. (2000) and follow earlier investigations for other sections of the oceanic crust (Staudigel et al., 1996). The composites are a series of samples that represent mixtures of all the major lithologies, primary igneous compositions and secondary compositions and characterize the large-scale compositional variation of the oceanic crust basement at Site 801. Special care was taken to include variably altered basalt (massive flows and pillows) together with vein material and interpillow hyaloclastites in these composites; these proportions were evaluated through core description and core-log reconstruction (Barr et al., 2002). For each basement unit (Units I, II and III), three composites were prepared, which included the volcanoclastic-rich lithologies (VCL), submarine extrusive (FLO) and the bulk basement section (MORB).

3. Methods

3.1. Major elements and ferric iron determination

Major element data were obtained from a 300-mg sample using ICP-atomic emission spectrometry fol-

lowing the procedure described by Govindaraju and Mevelle (1987); the precision for all elements is better than 2%. Additional data on major elements were obtained at Boston University (K. Kelley, personal communication). Ferrous iron (FeO) concentrations in the samples were determined by titration of a precision of 1–5%. Ferric iron concentrations are calculated as the difference between total iron (Fe_2O_{3T}) and ferrous iron concentrations.

3.2. Chemical purification of Fe isotopes

Aliquots of 50–100 mg of sample powder of a known Fe concentration were accurately weighed in PTFE beaker to obtain an equivalent of approximately 3 mg of Fe. The samples were then dissolved in 5 ml HF and 2 ml HNO_3. The acid solution was taken to dryness at 80 °C on a hot plate and then dissolved in 5 ml of 8N HCl in a heated (40 °C) closed vessel. A drop of H_2O_2 is added to the solution to oxidized any residual ferric iron. A precise volume of this solution corresponding to 2500 μg of Fe was then purified on Bio-Rad AG1-X8 anion resin (Vander Walt et al., 1985). Prior to chemical purification, 2 ml of resin was loaded in columns and was cleaned with 5 ml of 0.5N HNO_3 and 5 ml H_2O and conditioned by 5 ml of 8N HCl. After the sample solution was loaded on the resin, 10 ml of 8N HCl was passed through the column to remove the matrix and to strip other ions. The Fe was then eluted with 5 ml of 0.12N HCl. The purified samples were then diluted 100-fold (i.e., to 5 ppm) in HNO_3 0.01N prior to the analysis by mass spectrometry.

3.3. Fe-isotope mass spectrometry

$^{57}Fe/^{54}Fe$ ratios were determined with a Micromass Isoprobe MC-ICP-MS operating at CRPG-CNRS Nancy, France, using the instrumental settings given in Table 1. This instrument consists of a standard ICP source and magnetic mass analyzer, which incorporates an RF-only hexapole collision cell technology (Turner et al., 1998). By addition of small amounts of gas to the collision cell (such as Ar at few milliliters per minute, typically 1.8 ml/min), the interactions of ions from the plasma with the collision gas reduce the energy spread of the ions from 20 to 30 eV to less than 1 eV. It has been shown that this "collisional focusing" (Douglas and French, 1992) in an RF-only hexapole device induces a series of ion–molecule reactions between the gas and the ion beam allowing the removal of molecular ion interferences. The samples were introduced without the use of a peristaltic pump into the MC-ICP-MS via a PFA nebulier with a cyclonic spray chamber at a flow rate of 100 μl min^{-1}.

Table 1
MC-ICP-MS parameters

Instrument	Isoprobe, Micromass UK
RF power	1300 W
Argon flows (l min^{-1})	
Plasma gas	13.20
Auxiliary gas	1.20
Sample gas	0.48
Collision gas (Ar)	1.72
Hexapole vacuum	1.88×10^{-4} mbar
DAC	80%
Interfaces cones	Nickel
Ion lens setting	maximum intensity
Extraction potential	39%
Nebuliser	Low flow PFA nebuliser (100 μl min^{-1})
Admittance delay	120 s
Rinse delay	90 s
Raw data	20
Counting time	10 s

Iron has four isotopes ^{54}Fe(5.8%), ^{56}Fe(91.7%), ^{57}Fe (2.2%) and ^{58}Fe(0.28%), which have major interferences from ArN, ArO, ArOH and Ni, respectively. The hexapole collision cell technology using a mixture of Ar (at about 1.5 ml/min) and H (at about 0.8 ml/min) results in a decrease of the isobaric interference from ArO^+ and ArN^+ on ^{54}Fe and ^{56}Fe isotopes to a negligible level, below 0.1 mV. However, it was found that H enhances the formation of $ArOH^+$ (up to 10 mV), which is highly detrimental for the precise analysis of $^{57}Fe/^{54}Fe$. For routine analysis, we used only Ar as a collision gas (without H) as it was found that the contribution from ArN^+ and $ArOH^+$ at mass 54 and 57, respectively, was typically at the level of 1–5 mV corresponding to about 0.1–0.5% of the Fe ion beams when a Fe solution at a concentration of 5 ppm was analyzed. The correction of these interferences by on peak zero is explained in more detail below. A spectral interference on ^{54}Fe isotope from ^{54}Cr was found to be negligible both in

standard solution and in samples chemically purified and no correction for Cr interferences was required; nonetheless, the intensity of $^{52}Cr^{+}$ was monitored during each analysis.

The isotopic results are reported in the same manner as proposed for Fe, Cu and Se isotope measurements by MC-ICP-MS (Belshaw et al., 2000; Zhu et al., 2000a; Rouxel et al., 2002). This method involves the measurement of an internal standard (SPEX Fe elemental standard solution) between each sample yielding the isotopic composition of the sample expressed as a deviation relative to the standard following the equation

$$\delta^{57}\mathrm{Fe} = 1000 \times \left(\frac{R_{\mathrm{spl}}}{R_{\mathrm{std}}} - 1\right)$$

where R_{spl} is the measured $^{57}Fe/^{54}Fe$ ratio for the unknown sample and R_{std} is the mean $^{57}Fe/^{54}Fe$ ratio of the standard measured before and after the sample. Each data point given in this study corresponds to the mean of three replicate measurements of individual bracketed samples.

Because of the stability of the interferences from ArN^{+} and $ArOH^{+}$ at mass 54 and 57 using the same acid solution (HNO_3 0.01N) for diluting the standard and the samples, a correction was possible with <0.1‰ uncertainty. This correction involved the measurement of the acid solution in HNO_3 0.01N and subtracting the signal from both the matching standard and sample analysis (on peak zeros). The uncertainty was further minimized by matching the intensities of sample and standard to less than 10% difference. A blank solution was measured in 5 samples, and measurement runs were made using an autosampler generally including 10 samples and 12 matching standards and 2 blank solutions.

The internal precision of the measurements is evaluated by the measurement of the standard solution treated in the same way as for an unknown sample. Replicate measurements are presented in Fig. 3. The results show that measurements can be made at a precision better than 0.20‰ at 2σ level using this procedure.

3.4. External reproducibility

Because Fe isotopes can be fractionated during column chromatography (Anbar et al., 2000), we verified that the yield for Fe purification was complete. Using Fe contents determined by ICP-AES, and by comparing the Fe concentration on aliquots drawn before and after anion exchange column, we obtained a yield of 105% ± 7% for all samples. Furthermore, we measured the Fe concentration in several sample solutions passed through AG1-X8 in HCl 8N. Under these conditions, Fe is retained on the resin and the eluted solution contain all other major elements, including Na, Ca, Al, Ti, K and Mg. The concentration of Fe in this eluted solution is less than 1% of the

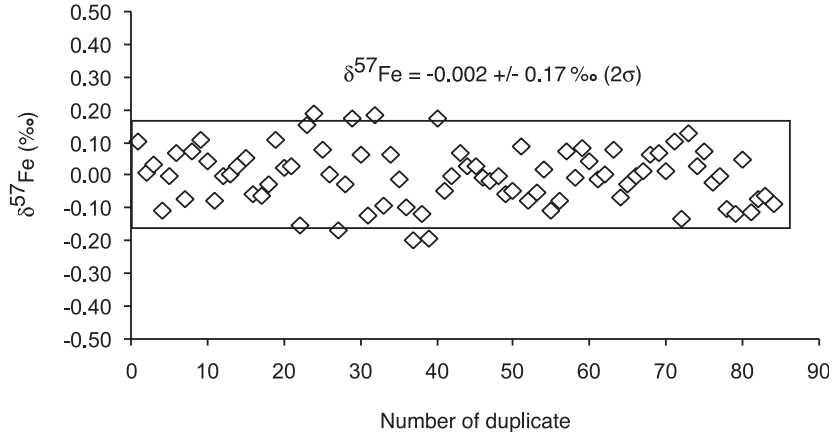

Fig. 3. δ^{57}Fe of internal standard (SPEX element Fe solution) over different analytical sessions (8-month period). The internal precision of our δ^{57}Fe measurements is estimated to be 0.17‰ at 2σ level based on 84 duplicates.

initial Fe concentration of the sample, showing that the chemical yields of better than 99%.

As sample matrix may affect instrumental mass bias and create complex isobaric interferences in the MC-ICP-MS, we verified that a single pass through an ion exchange column was sufficient to reduce sample matrix to the purity of the standard by using four experiments: (1) measurement of the sample solution for major element chemistry; (2) duplicated purification through AG1-X8; (3) verification that Fe isotopic variations were only attributed to mass fractionation line by measuring $^{56}Fe/^{54}Fe$ ratio in addition to $^{57}Fe/^{54}Fe$ ratio (4) measurement of a standard solution doped with various matrices.

For experiment (1), all major matrix elements (Si, Al, Mn, Ca, Na, K, Ti, P, Mg) measured by ICP-AES were found to be <1% of the total Fe. The results of experiments (2) show within error that there is no shift between single and double pass through chromatographic column (Table 2). Experiment (3) was undertaken during two different sessions on the MC-ICP-MS, as the measurement of $^{56}Fe/^{54}Fe$ requires the use of H in addition to Ar in the collision cell and does not allow a simultaneous precise measurement of $^{57}Fe/^{54}Fe$. Identical results within error for key samples of this study having either different matrix composition or Fe-isotope composition confirm that the $^{57}Fe/^{54}Fe$ variations determined are due to mass fractionation by natural processes (Fig. 4). For experiment (4), several samples defining a large spread of Fe-isotope variations and/or matrix compositions were used. Fe was removed after purification through AG1-X8 and standard solution IRMM-14 added to this Fe-free sample matrix and processed through chemical purification described above. The isotopic compositions of these synthetic samples are identical to the isotopic composition the ultra-pure IRMM-14 standard solution (Table 2).

Table 2
Duplicated separation through anion-exchange resin

Sample	$\delta^{57}Fe_{IRMM-14}$		$\Delta^{57}Fe$
	1× AG1-X8	2× AG1-X8	
801C-9R1,32	−0.78	−0.53	−0.25
1149B-29R2,7	1.04	0.94	0.10
1149B-18R1,97	−0.23	−0.40	0.17
801C-4R1,1	−2.37	−2.48	0.11
1149B-31R1,114	0.14	0.28	−0.14
IRMM-14 + 1149B-29R2,7	0.06[a]	n.d.	
IRMM-14 + 1149B-1W1,113	−0.01[a]	n.d.	
IRMM-14 + 801C-15R7,1/D	0.05[a]	n.d.	
IRMM-14 + BHVO-1	0.13[a]	n.d.	

IRMM-14 was doped with sample matrix (Fe was removed through AG1-X8). Fe concentration in synthetic sample is 1–2 wt.% n.d. not determined.

[a] Data performed on Nu Plasma MC-ICP-MS (Nu Instrument, UK) at Cambridge University, UK.

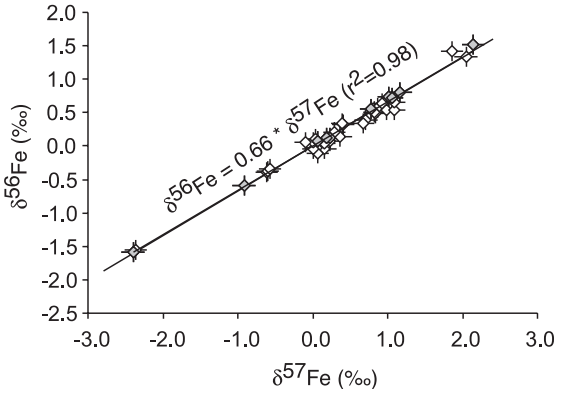

Fig. 4. $\delta^{57}Fe-\delta^{56}Fe$ plot showing mass-dependant variation of Fe isotope in a selected set of samples. Data obtained on the Isoprobe (open diamond) with $\delta^{57}Fe$ and $\delta^{56}Fe$ analyzed separately and Nu Plasma (gray diamond) with $\delta^{57}Fe$ and $\delta^{56}Fe$ analyzed simultaneously.

Several georeference materials (Govindaraju, 1994) of igneous rocks and Fe-isotope reference standard IRMM-014 were analyzed for their Fe isotopic composition relative to our internal Fe isotopic standard SPEX and converted relative to IRMM-14 (Table 3). We obtained for BIR-1, BR, BE-N, BCR-1 and BHVO-1, $\delta^{57}Fe$ values of 0.06‰, 0.12‰, 0.18‰, 0.08‰, 0.22‰, respectively, suggesting that the upper mantle reservoir has a value of 0.13 ± 0.17‰ relative to IRMM-14. This baseline is thus indistinguishable from the average of lunar and terrestrial igneous rocks defined at $\delta^{57}Fe = 0.14 \pm 0.08$‰ (relative to IRMM-14) by Beard et al. (2003). All data in this study are hereafter reported relative to the international Fe isotopic standard IRMM-14.

Table 3
δ^{57}Fe composition of georeference materials (igneous material) and IRMM-14

Standard	No.	$\delta^{57}Fe_{SPEX}$	$\delta^{57}Fe_{IRMM-14}$	2 s.d.
BCR-1: Columbia	1	0.18	− 0.01	
River Group basalt,	2	0.26	0.07	
USA (USGS)	3	0.26	0.07	
	4	0.38[a]	0.19[a]	
	mean	0.27	0.08	0.10
BE-N: Basalt,	1	0.35	0.16	
France (IWG-GIT)	2	0.39	0.20	
	mean	0.37	0.18	0.06
BIR-1: Icelandic	1	0.25[a]	0.06[a]	
basalt (USGS)				
BHVO-1: Hawaiian	1	0.36	0.17	
basaltic lava,	2	0.45	0.26	
USA (USGS)	3	0.42[a]	0.23[a]	
	mean	0.41	0.22	0.13
BR: Basalt,	1	0.45	0.26	
France (CRPG)	2	0.32	0.13	
	3	0.23	0.04	
	4	0.21	0.02	
	5	0.32	0.13	
	6	0.22	0.03	
	7	0.21	0.02	
	8	0.22	0.03	
	9	0.32	0.13	
	10	0.29	0.10	
	11	0.38	0.19	
	12	0.50	0.31	
	mean	0.31	0.12	0.19
Terrestrial Igneous		0.32	0.13	0.17
Rocks—average				
IRMM-14:	1	0.15		
Certified Isotopic	2	0.07		
Reference Material	3	0.27		
(Institute for	4	0.26		
Reference Materials	5	0.23[a]		
and Measurements)	6	0.11[a]		
	7	0.21[a]		
	mean	0.19	0.00	0.19

[a] Data performed on Nu Plasma MC-ICP-MS (Nu Instrument, UK) at Cambridge University, UK.

Based on a duplicate analysis of samples and standards processed through chemistry (Tables 3 and 4), we record an external precision of 0.20‰ (2σ level) for the analyses presented in this study.

4. Results

The descriptions of the sediments and basalts are given in Tables 5, 6 and 7, together with the δ^{57}Fe values and major element determinations. For Site 801, the studied samples cover the major lithologies recovered at this site along a 900-m profile through the oceanic crust, and individual δ^{57}Fe data are shown in Fig. 5. The Fe-isotope composition of composite samples at Site 801 and the representative δ^{57}Fe results (i.e., range and average) for the main lithologies in the oceanic crust (Sites 801, 1149 and 765) are summarized in Table 8. The preliminary results show that all major lithologies have similar bulk Fe-isotope compositions that are very close to that of igneous value, which is defined at 0.13 ‰ relative to IRMM-14 (Table 3; Beard et al., 2003). However, discrete analysis of altered rocks and veins revealed that Fe isotopes are heterogeneously distributed with the oceanic crust as described below.

4.1. Deep-sea sediments

Deep-sea clays and volcanoclastites have a restricted Fe isotopic composition clustered around the igne-

Table 4
Duplicated chemical purification and δ^{57}Fe analysis

Sample	$\delta^{57}Fe_{IRMM-14}$	$\delta^{57}Fe_{IRMM-14}$ ditto	$\Delta^{57}Fe_{IRMM-14}$
1149B-29R2,7	1.04	1.14	− 0.10
ditto		1.02[a]	0.02
1149B-31R1,114	0.14	0.09	0.05
1149C-1W1,113	− 0.48	− 0.52	0.04
801 SUPER	0.12	0.04	0.07
801B-20R1,12	− 0.19	− 0.14	− 0.05
801C-12R1,48	− 0.55	− 0.60	0.05
801C-15R7,1/D	2.05	2.12	− 0.07
ditto		2.14[a]	− 0.09
801C-15R7,1/V	− 0.53	− 0.62	0.09
801C-15R7,31	0.99	1.09	− 0.10
ditto		1.17[a]	− 0.18
801C-16R3,54	0.36	0.28	0.08
801C-16R3,82-87	0.74	0.84	− 0.10
801C-22R1,7	− 0.52	− 0.57	0.05
801C-43R2-75-79/V	1.64	1.86	− 0.22
801C-4R1,1	− 2.23	− 2.37	0.14
ditto		− 2.40[a]	0.17
801C-5R1,95	0.82	1.08	− 0.26
801C-6R3,18	0.72	0.67	0.05
ditto		0.86[a]	− 0.14
801C-6R3,42	− 0.09	0.13	− 0.22
801C-9R1,32	− 0.61	− 0.78	0.17
ditto		− 0.72[a]	0.11

ditto: duplicated analysis.
[a] Data performed on Nu Plasma MC-ICP-MS (Nu Instrument, UK) at Cambridge University, UK.

ous δ^{57}Fe values (between −0.07‰ and 0.23‰, Table 5). This is consistent with the Fe-isotope compositions of loess (δ^{57}Fe values between −0.06‰ and 0.48‰), which has been used to infer the Fe-isotope composition of the upper continental crust (Zhu et al., 2000b). In contrast, deep-sea cherts display significantly larger Fe-isotope variations with δ^{57}Fe being more negative relative to igneous δ^{57}Fe values (between −0.48‰ and 0.06‰, Table 5). Using our data set of 15 samples, we calculated an average of 0.06‰ for deep-sea clay and volcanoclasites and −0.11‰ for cherts (Table 8). As these lithologies comprise the major part of deep-sea sediments, our results suggest that the average δ^{57}Fe value for the entire sedimentary section of the oceanic crust is similar to or slightly lower than the igneous value. However, minor lithlogies such as carbonate-rich sediments (chalks) have δ^{57}Fe significantly less than igneous value (down to −1.12‰, Table 5), which are similar to the δ^{57}Fe values in Fe–Mn nodules from the ocean basins (Beard and Johnson, 1999; Zhu et al., 2000b). In these carbonate-rich samples, Fe is believed to be present in the form of hydrogenous ferromanganese precipitates, which may provide a record of Fe dissolved in seawater (Zhu et al., 2000b). Our study confirms therefore the general observation that terrigenous sources of Fe are not fractionated relative to the upper mantle, whereas chemically precipitated Fe is significantly shifted toward negative values, probably reflecting a fractionated source of Fe in seawater.

4.2. Interflow materials, volcanoclasites and veins

Interpillow sediments display a large range of Fe-isotope variation, which contrasts strongly with the relative homogeneity of δ^{57}Fe values in deep-sea sediments (Tables 6 and 7). The overall variation recorded in interpillow sediments, which include the Si–Fe-rich hydrothermal deposits, range from highly negative δ^{57}Fe values of as low as −2.5‰ (sample 801C-04R1,1) to positive values as much as 1.0‰ (sample 1149B-29R2,7). Two types of interpillow sediments have been studied and include carbonate-rich sediments, in the form of small discrete infillings in cavities between lava flows and silica-rich sediments, which may form thick hydrothermal deposit units (>1 m) intercalated between lava flows (Site 801).

In Si–Fe-rich hydrothermal deposits, Fe occurs predominantly as Fe oxhydroxide with $Fe^{3+}/\Sigma Fe>0.9$, suggesting that iron is almost completely oxidized. In these samples, δ^{57}Fe values range from values slightly higher than igneous values (0.39‰) to negative values (−0.52‰), suggesting heterogeneity of Fe isotopes in these samples. Furthermore, one chert sample situated just above the hydrothermal deposits yields the lowest δ^{57}Fe value down to −2.49‰. In this sample, Fe is depleted tenfold relative to typical Si–Fe-rich hydrothermal deposits (ΣFe = 0.7 wt.%). The close proximity to the hydrothermal deposits and the large Fe-isotope fractionation relative to other deep-sea cherts suggest that this sample has been strongly influenced by the past hydrothermal activity of the section of this crust.

In carbonate-rich interpillow sediments, $Fe^{3+}/\Sigma Fe$ values vary from 0.2 to 0.9, and mineralogical examination and chemical composition (high MgO and low K_2O contents) suggest that that Fe occurs as smectite, probably saponite (Andrews, 1980) and Fe oxyhydroxides (e.g., samples 1149B-29R2,7 and 801C-9R1,32). Despite the fact that the Fe phases are derived mainly from basalt alteration, it is important to stress the large variation of δ^{57}Fe observed in these samples, with δ^{57}Fe values being both lower and higher than the igneous value (from −0.78‰ to 1.04‰).

Similar features have been also obtained for veins and volcanoclastic materials recovered downhole at Sites 801C, 1149 and 765. This material displays a large range of Fe content and $Fe^{3+}/\Sigma Fe$ suggesting that Fe is easily mobilized, variably oxidized and redeposited within altered lava flows and along open cracks in the oceanic crust. Secondary pyrite recovered from veins tends to have negative δ^{57}Fe values (δ^{57}Fe from −1.07‰ to 0.01‰) relative to adjacent basalt. Large deviations in Fe-isotope composition relative to fresh basalts are observed for volcanoclasites and clay-rich veins (from −0.55‰ to 1.86‰). As this material is composed of clasts of altered basalts, secondary minerals such as smectite and celadonite, and a matrix of carbonate and sediments in various proportions, its Fe-isotope composition represents a mixture of the different δ^{57}Fe end-members. Despite the fact that there are no clear relationships between sample chemistry and Fe-isotope composition, the celadonitic-rich samples (such as 801C-43R2, 75/V) yield the highest δ^{57}Fe values (1.86‰) suggesting that in

Table 5
Descriptions and chemical and Fe-isotope compositions of sediments at Sites 1149 and 801

Sample	Depth (m)	Unit	LOI	Al_2O_3	CaO	Fe_2O_{3T}	FeO	K_2O	MgO	MnO	Na_2O	P_2O_5	SiO_2	TiO_2	SUM	$\delta^{57}Fe$	Description
1149B-06R1,38	199.1	CT	4.16	2.08	0.30	1.77	< 0.05	0.50	0.57	0.09	0.36	0.14	89.70	0.11	99.8	− 0.08	Deep-sea chert
1149B-18R1,97	302.6	CT	13.54	1.78	14.15	1.53	–	0.53	0.73	0.11	0.52	0.07	66.80	0.09	99.85	− 0.23	Carbonate-rich sediment with fine grained quartz, horizontal layers
1149B-22R1,106	341.2	CT	2.31	1.36	< 0.05	0.95	< 0.05	0.36	0.29	< 0.05	0.16	< 0.05	94.16	0.05	99.64	− 0.23	Red-brown chert with irregular banding, including minor carbonate
1149B-27R1,49	388.0	CK	40.58	0.86	50.11	1.42	–	0.31	1.09	0.13	0.30	< 0.05	5.07	< 0.05	99.87	− 1.12	Nannofossil chalk with light reddish brown clays, laminated
1149C-01W1,113	–	CT	2.43	0.60	< 0.05	0.46	–	0.18	0.16	< 0.05	0.16	< 0.05	95.61	< 0.05	99.6	− 0.48	Light brown chert
1149C-05R1,19	303.0	CT	2.66	1.02	0.33	0.86	–	0.31	0.31	0.14	0.19	0.05	93.85	0.05	99.8	− 0.28	Dark brown chert
1149C-09R1,37	398.3	CK	41.88	0.58	52.17	0.88	< 0.05	0.23	0.57	0.32	0.17	< 0.05	3.01	< 0.05	99.8	− 0.31	Light brown chalk with micro Mn nodules
1149D-04R1,43	291.3	CT	2.28	1.12	0.85	0.80	–	0.30	0.30	0.07	0.16	< 0.05	93.80	< 0.05	99.7	− 0.20	Light brown chert
801A-03R2,145	15.0	DSC	11.43	16.82	1.85	7.34	< 0.05	2.30	3.27	2.15	2.09	1.04	49.56	0.61	98.5	0.01	Dark brown deep sea clays

801A-05R3,145	36.1	DSC	10.51	15.13	1.75	6.04	–	1.50	2.97	0.96	2.09	0.98	54.46	0.55	96.9	0.04	Dark brown deep sea clays
801A-19R1,65	167.4	DSC	9.24	6.76	4.76	6.40	–	0.60	3.67	0.08	1.97	0.26	63.62	1.36	98.7	0.23	Dark green deep sea clay
801B-02R1,117	196.7	DSC	10.71	10.09	3.58	10.47	2.38	0.93	12.94	0.20	3.36	0.33	45.65	2.24	100.5	0.07	Volcanoclastic silty sandstone
801B-20R1,12	374.6	CT	2.35	1.49	0.18	0.94	–	0.34	0.31	0.17	0.25	0.09	93.61	0.06	99.8	−0.19	Dark brown chert
801B-27R1,62	415.3	CK	4.89	4.39	0.33	3.40	<0.05	1.23	1.16	0.69	0.85	0.10	82.70	0.21	100.0	−0.49	Chalk light brown-cream colored with micro Mn nodules, very fine grained
801B-31R1,33	433.9	CT	2.63	1.65	0.18	1.28	–	0.43	0.33	0.25	0.28	0.09	92.61	0.08	99.8	0.06	Dark brown to yellowish red chert, unmineralized fractures
801B-35R2,0	445.8	DSC	7.46	8.60	0.48	10.50	<0.05		2.15	0.10	1.41	0.24	64.35	0.61	95.9	−0.07	Claystone
801B-37R1,13	461.7	CT	1.52	1.26	0.08	1.72	–	0.19	0.14	0.04	0.08	0.02	97.41	0.03	98.5	0.24	Red/brown chert
801B-40R1,2	476.9	CT	0.74	0.22	<0.05	1.04	–	0.06	<0.05	<0.05	<0.05	<0.05	98.02	<0.05	100.1	0.24	Dark brown chert 40% with 60% crystallized quartz

CT: deep-sea chert; CK: carbonate-rich sediments (chalk), DSC: deep-sea clays.
δ^{57}Fe values reported relative to international standard IRMM-14 (‰).

Table 6
Descriptions and chemical and Fe-isotope compositions of basalts at Sites 1149 and 765

Sample	Depth (m)	Type	LOI	Al_2O_3	CaO	Fe_2O_{3T}	FeO	K_2O	MgO	MnO	Na_2O	P_2O_5	SiO_2	TiO_2	Sum	δ^{57}Fe	Description
1149B-29R1,66	407.5	IFM	17.0	8.9	5.3	10.1	0.2	1.2	9.0	0.1	1.2	0.1	45.8	1.1	100.0	0.47	Clay-rich interpillow sediment
1149B-29R2,120	409.5	IFM	1.9	14.3	10.9	14.0	–	0.5	6.5	0.2	2.5	0.2	47.3	1.7	99.8	− 0.22	Si- and Fe-rich vein, (chert material filling)
1149B-29R2,7	408.4	IFM	34.4	1.0	39.9	13.6	0.4	0.1	3.4	0.2	0.2	0.1	7.2	0.1	100.3	1.04	Carbonate- and Fe-rich sediment. Heterogenously colored
1149B-29R3,60/D	410.3	FLO	2.1	15.4	11.1	7.9	4.6	0.2	7.9	0.1	2.7	0.2	50.3	1.8	104.5	0.16	Light grey basalt (diabase) with minor mottled patches, least altered
1149B-29R3,60/H	410.3	FLO	3.4	14.4	10.2	13.0	4.7	0.8	6.1	0.2	2.5	0.2	47.4	1.7	104.6	0.22	Dark green and brown basalt halo with thin Fe-oxyhydroxide veinlet
1149B-31R1,114	427.1	VCL	14.3	12.7	1.6	12.3	1.0	2.9	7.0	0.1	1.5	0.1	46.1	1.3	100.8	0.28	Hyaloclastite, smectite and carbonate matrix with clasts of altered basalt
1149C-11R1-19-23/D	417.2	FLO	2.0	15.1	11.1	9.8	4.4	0.3	7.7	0.2	2.6	0.2	49.2	1.6	104.2	0.15	Light grey basalt (diabase), pervasively altered
1149C-11R1-19-23/H	417.3	FLO	2.5	14.1	11.1	13.0	4.8	1.0	6.2	0.2	2.4	0.2	47.8	1.5	104.6	0.15	Dark green basalt halo with thin rim of Fe-oxyhydroxides

1149D-07R1,37	320.1	VCL	–	–	–	–	–	–	–	–	–	–	–	–	–	0.48	Hyaloclastite, smectite and carbonate matrix with clasts of altered basalt
1149D-07R2-20-25/D	321.4	FLO	1.9	15.5	11.0	7.8	4.5	0.2	7.9	0.1	2.9	0.2	50.5	1.8	104.4	0.04	Light grey aphyric basalt (diabase) with mottled pattern
1149D-07R2-20-25/H	321.4	FLO	1.7	14.8	10.3	12.7	4.7	0.8	6.2	0.2	2.7	0.2	48.6	1.7	104.6	0.18	Dark green basalt halo with minor brown tint from Fe-oxides
765D-18R1,44/D	1102	FLO	1.7	14.9	11.7	10.0	5.1	0.6	6.6	0.2	2.5	0.2	50.2	1.4	104.9	0.06	Light grey altered basalt (diabase), microdolerite
765D-18R1,44/H	1102	FLO	1.8	14.2	11.3	14.3	5.8	0.5	6.3	0.2	2.4	0.2	47.5	1.3	105.7	0.07	Dark green and brown halo
765D-23R1,137/D	1149	FLO	1.3	14.9	12.0	9.7	5.6	0.6	6.0	0.2	2.8	0.2	50.1	1.6	104.7	-0.02	Fine grained, grey mottled basalt (diabase)
765D-23R1,137/H	1149	FLO	1.6	14.2	11.0	16.1	6.0	0.5	5.6	0.2	2.6	0.2	46.4	1.5	105.7	0.06	Red-green halo well developed
765D-7R3,6/D	1005	FLO	2.5	15.4	14.2	8.0	4.8	0.3	6.4	0.2	2.8	0.2	48.2	1.3	104.2	0.37	Light grey altered basalt (diabase)
765D-7R3,6/H	1005	FLO	2.6	13.2	12.1	15.2	5.7	0.7	6.1	0.2	2.3	0.1	46.2	1.1	105.5	0.01	Dark green basalt halo

IFM: interflow materials; VCL: volcanoclastites including hyaloclasites and breccia; FLO: altered basalts.
δ^{57}Fe values reported relative to international standard IRMM-14 (‰).

Table 7
Descriptions and chemical and Fe-isotope compositions of samples at Site 801C

Sample	Depth (m)	Type	Unit	LOI	Al_2O_3	CaO	Fe_2O_{3T}	FeO	K_2O	MgO	MnO	Na_2O	P_2O_5	SiO_2	TiO_2	SUM	$\delta^{57}Fe$	Description
801C-04R1,1	521.7	IFM	H.D. I	2.84	0.17	1.78	1.06	–	< 0.05	0.65	0.12	< 0.05	< 0.05	93.19	< 0.05	99.8	− 2.49	Red brown chert with recrystallized quartz
801C-04R1,72	522.4	IFM	H.D. I	2.40	0.58	0.03	12.78	–	0.01	0.06	0.01	0.12	0.02	85.63	0.00	97.6	0.39	Si–Fe-rich hydrothermal deposit
801C-04R2,19	523.3	IFM	H.D. I	2.12	< 0.05	0.10	11.98	–	< 0.05	< 0.05	< 0.05	0.11	0.07	85.24	< 0.05	99.6	− 0.01	Si–Fe-rich hydrothermal deposit including pure quartz patches (medium porosity)
801C-05R1,95	532.2	FLO	Unit I	9.77	19.63	4.97	5.94	0.67	8.10	2.17	0.05	1.46	0.09	57.38	1.04	111.3	0.82	Green altered basalt, (celadonite-rich)
801C-05R1,110	532.3	IFM	Unit I	33.57	2.75	35.02	7.85	1.33	1.77	3.82	0.52	0.25	< 0.05	14.37	< 0.05	101.3	− 0.09	Sediment including clay-rich material (80%) with Si–Fe-rich hydrothermal components (20%)
801C-5R3, 80	534.6	FLO	Unit I	5.20	23.03	10.42	4.39	–	0.73	1.57	0.04	3.20	0.11	55.34	1.24	100.1	0.78	Highly altered pale–green pillow margin
801C-06R3,18	543.5	FLO	Unit I	6.42	22.06	7.97	3.63	0.96	2.56	1.67	< 0.05	2.72	0.07	51.55	1.19	100.8	0.78	Light green–brown very altered aphyric basalt
801C-06R3,42	543.7	FLO	Unit I	11.85	21.89	14.07	6.01	2.57	0.83	2.39	0.15	3.04	0.07	50.00	1.08	114.0	0.13	Altered basalt with small calcite vein
801C-08R1,46	560.0	VCL	Unit I	14.54	10.31	12.71	14.14	5.91	2.12	3.34	0.18	1.87	0.15	39.11	1.34	99.8	0.10	Breccia with 35% of matrix composed of carbonate, Fe-oxyhydroxides and green clays (celadonite)
801C-09R1,32	563.5	IFM	Unit I	36.96	0.82	33.09	12.88	9.26	< 0.05	6.03	0.77	0.21	< 0.05	9.00	0.05	109.1	− 0.78	Sediment with red chert with carbonate and recrystallized quartz
801C-10R6,71	576.9	IFM	Unit I	27.57	3.72	39.49	9.79	4.12	0.06	7.43	0.96	0.81	0.05	36.86	0.34	131.2	− 0.55	Sediment with red chert with carbonate and recristallized quartz in contact with quench pillow margin

801C-12R1,48	587.8	VCL	Unit I	18.63	3.27	16.32	12.62	1.82	3.25	5.42	0.28	0.55	< 0.05	39.18	0.23	101.6	− 0.55	Hyaloclastite with celadonite 70% and carbonate 20%. 10% of highly altered glass (chilled margin)
801C-15R2,117	616.2	FLO	Unit II	8.18	17.21	9.60	10.89	4.14	0.52	4.27	0.09	3.51	0.22	49.89	2.10	110.6	0.71	Light green altered pillow
801C-15R4,60	618.3	FLO	Unit II	4.67	14.76	10.98	12.56	7.42	0.11	5.74	0.16	2.79	0.20	46.05	1.85	107.3	0.02	Grey altered basalt, medium grained with thin veins of smectites
801C-15R5,66	619.7	FLO	Unit II	3.44	14.06	11.72	14.55	8.72	0.04	6.38	0.21	2.78	0.16	48.07	1.73	111.9	0.16	Minimally altered basalt
801C-15R7,1/D	621.4	FLO	Unit II	7.10	19.45	8.15	5.45	0.83	0.86	1.51	0.03	3.65	0.20	50.99	2.44	100.7	2.05	Highly altered basalt, light green sage colored
801C-15R7,1/V	621.4	IFM	Unit II	35.90	0.94	25.17	9.62	6.32	0.37	11.68	0.43	0.11	< 0.05	16.13	< 0.05	106.7	− 0.62	Interpillow sediment red carbonate- and Fe-rich material
801C-15R7,31	621.7	FLO	Unit II	10.97	20.42	14.26	5.65	1.67	0.53	2.02	0.15	3.82	0.27	51.10	2.41	113.3	1.09	Sage, bleached basalt
801C-16R2,82	625.6	FLO	Unit II	11.73	18.50	12.67	8.41	2.85	0.73	2.60	0.14	3.41	0.27	48.77	2.68	112.8	0.41	Sage, bleached basalt
801C-16R3,29	626.3	IFM	H.D. II	2.86	< 0.05	< 0.05	20.59	–	< 0.05	< 0.05	< 0.05	0.05	< 0.05	76.06	< 0.05	99.6	− 0.12	Si–Fe-rich hydrothermal deposit
801C-16R3,54	626.6	IFM	Unit II	33.99	0.70	24.82	13.33	8.35	0.80	9.16	0.35	0.08	< 0.05	16.49	0.07	108.1	0.28	Interpillow sediment, green clay 15%+ carbonate 80%+red layer of chert 5%
801C-16R3,82	626.8	FLO	Unit II	8.28	16.57	6.18	12.13	5.62	0.45	2.51	0.10	3.19	0.38	45.34	3.78	104.5	0.74	Light green highly altered basalt (sage alteration)
801C-16R4,9	627.5	VCL	Unit II	–	–	–	–	–	–	–	–	–	–	–	–	–	− 1.07	Pyrite vein (hand-picked)
801C-17R1,100	633.8	FLO	Unit II	3.08	12.72	11.26	15.90	10.04	0.08	5.48	0.26	2.53	0.28	46.06	2.71	110.4	0.02	Dark grey (least) altered basalt with secondary pyrite and carbonate patches

(continued on next page)

Table 7 (*continued*)

Sample	Depth (m)	Type	Unit	LOI	Al_2O_3	CaO	Fe_2O_{3T}	FeO	K_2O	MgO	MnO	Na_2O	P_2O_5	SiO_2	TiO_2	SUM	$\delta^{57}Fe$	Description
801C-22R1,7	673.7	IFM	H.D. II	2.39	0.25	0.11	13.12	0.20	< 0.05	0.10	< 0.05	< 0.05	< 0.05	83.69	< 0.05	99.9	− 0.52	Si–Fe-rich hydrothermal deposit with chert-like layers (very low porosity)
801C-34R3,81/B	788.8	FLO	Unit III	3.35	12.85	9.39	16.24	5.11	0.70	5.30	0.18	2.59	0.22	46.70	2.33	105.0	− 0.30	Altered basalt including large brown alteration halo
801C-34R3,81/V	788.8	VCL	Unit III	11.74	2.10	4.85	42.60	2.16	3.09	4.27	0.07	0.33	< 0.05	31.28	< 0.05	102.5	− 0.19	Large celadonite and Fe-oxyhydroxide vein
801C-37R1,83/D	814.1	FLO	Unit III	3.47	13.29	10.50	13.71	6.89	< 0.05	6.00	0.22	2.65	0.25	47.53	2.34	106.9	0.11	Vesicular basalt with void filled with carbonate and saponite
801C-37R1,83/V	814.1	VCL	Unit III	10.81	6.24	2.04	46.84	9.08	0.50	4.76	0.07	0.47	0.11	27.48	1.02	109.4	0.32	Large celadonite and Fe-oxyhydroxide vein with minor carbonate
801C-37R3,30	816.2	VCL	Unit III	–	–	–	–	–	–	–	–	–	–	–	–	–	−0.18	pyrite vein (hand-picked)
801C-37R5,30	818.8	VCL	Unit III	–	–	–	–	–	–	–	–	–	–	–	–	–	− 0.01	pyrite vein (hand-picked)
801C-39R2,28	834.0	FLO	Unit III	1.88	13.80	10.77	14.18	7.30	0.07	6.85	0.27	2.62	0.23	46.83	2.34	107.1	− 0.02	Grey aphyric basalt, least altered
801C-43R1,29	860.2	VCL	Unit III	–	–	–	–	–	–	–	–	–	–	–	–	–	−0.37	Pyrite vein (hand-picked)
801C-43R2,75/D	871.3	FLO	Unit III	0.25	14.58	10.74	12.69	6.78	0.20	6.53	0.22	3.02	0.26	48.57	2.10	105.9	− 0.22	Altered basalt with thin veins
801C-43R2,75/V	871.3	VCL	Unit III	5.23	2.32	0.45	25.33	3.76	8.93	6.93	< 0.05	0.19	< 0.05	50.17	0.06	103.4	1.86	Pure celadonitic vein with minor Fe-oxyhydroxides

IFM: interflow materials; VCL: volcanoclastites including hyaloclasites and breccia; FLO: altered basalts.
$\delta^{57}Fe$ values reported relative to international standard IRMM-14 (‰).

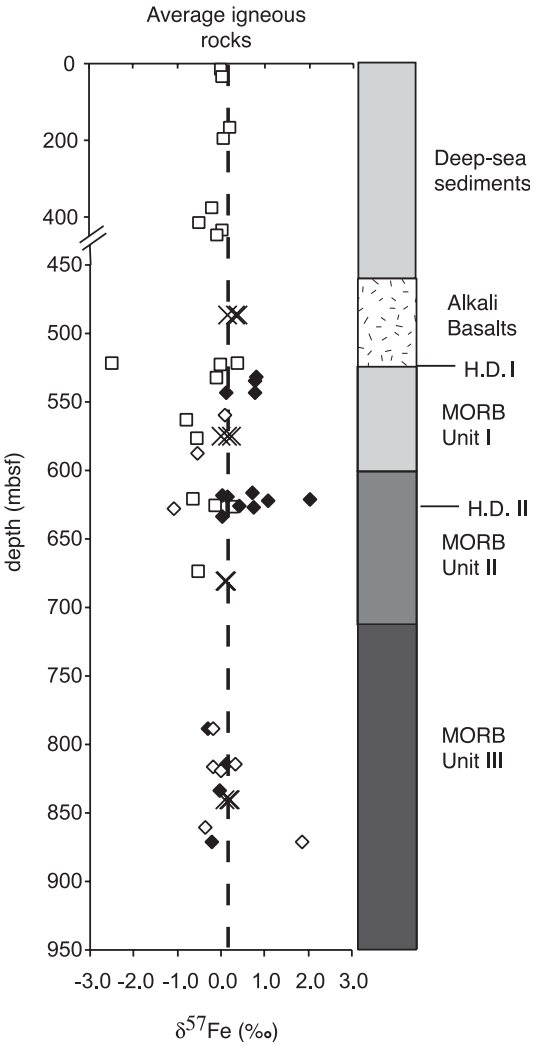

Fig. 5. A simplified stratigraphic section (in meters below seafloor, mbsf) through the first 1000 m of Jurassic oceanic crust at ODP Site 801C showing the major lithologies encountered. δ^{57}Fe values are shown for the deep-sea sediments and interpillow sediments including the Si–Fe-rich hydrothermal deposits (□), altered basalts (♦), breccia, hyaloclastites and vein materials (◇) and composite samples (weighted mixtures over a depth interval) (X). H.D: Si–Fe hydrothermal deposits intercalated between lava flows.

some cases, Fe-isotope signatures may be controlled by mineralogy.

The δ^{57}Fe value of the interflow sediment composite (a weighted mixture of the sediment components of the basement section, Table 8) suggests that, despite the variation between individual samples, the bulk sediment composition is very close to the igneous value. For volcanoclastic composites (VCL), the δ^{57}Fe values range from −0.01 ‰ to 0.13 ‰, which is similar to initial fresh rocks (δ^{57}Fe around 0.17 ‰).

4.3. Altered basalts

The δ^{57}Fe values of the lava flow composite samples (FLO) do not vary within error (Table 8)

Table 8
Summary of Fe isotopic composition of major lithologies recovered at Site 801

Sample type, major lithologies	δ^{57}Fe (‰), range	δ^{57}Fe (‰), bulk
Silica-rich sediments (chert)	−0.48 to 0.23 ($n=10$)	−0.11[a]
Deep-sea clay + volcanoclastites	−0.07 to 0.23 ($n=5$)	0.06[a]
Interpillow sediment (including hydrothermal deposit)	−2.49 to 1.04 ($n=13$)	−0.25[a]
Alkalic basalt VCL	n.d.	0.06[b]
Alkalic basalt FLO	n.d.	0.33[b]
Alkalic basalt		0.39[b]
Tholeitic basalt (Unit I) FLO	0.13 to 0.82 ($n=3$)	0.23[b]
Tholeitic basalt (Unit I) VCL	−0.55 to 0.20 ($n=2$)	−0.01[b]
Tholeitic basalt (Unit I) MORB		0.15[b]
Tholeitic basalt (Unit II) FLO	0.02 to 2.05 ($n=8$)	0.12[b]
Tholeitic basalt (Unit II) VCL	−1.07 ($n=1$)	0.08[b]
Tholeitic basalt (Unit II) MORB		0.13[b]
Tholeitic basalt (Unit III) FLO	−0.30 to 0.11 ($n=3$)	0.19[b]
Tholeitic basalt (Unit III) VCL	−0.37 to 1.86 ($n=6$)	0.09[b]
Tholeitic basalt (Unit III) MORB		0.22[b]
Bulk oceanic crust Site 801-1149-765	−1.07 to 2.05	0.12[b]
Grand average	($n=38$)	0.23[a]

n.d.: not determined.
VCL: composite of volcanoclastic material, including veins (pyrite, celadonite, Fe-oxhydroxide).
FLO: composite of altered basalts, including pillows and massive flows.
MORB: composite of altered oceanic crust including pillows, massive flows and volcanoclasites.
[a] Mean of Fe isotopic composition.
[b] Composite sample analysis.

with values between 0.12 ‰ and 0.23 ‰, which is in marked contrast to the variation of 4 ‰ observed for discrete samples from the basement section. Of particular interest is that at Site 801C, Fe isotopes display highly positive δ^{57}Fe values (up to 1.95 ‰) in highly altered basalts, which, in general, is in contrast to the negative values (down to −2.47 ‰) in alteration products such as pyrite veins and hydrothermal deposits.

Basalts from Units I and II at Site 801 underlying the Fe–Si hydrothermal deposits are intensely leached in Fe (ΣFe varies from 11 to 2 wt.%) and are highly oxidized relative to fresh basalt with $Fe^{3+}/\Sigma Fe$ ranging from 0.30 to 0.86. As shown in Fig. 6a, Fe^{2+} and ΣFe are highly correlated in MORB Units I and II and follow a relationship that is close to unity which suggests that the variation of ΣFe during alteration is controlled by the selective leaching of Fe^{2+}. Consequently, the increase in $Fe^{3+}/\Sigma Fe$ in these rocks is probably due to the selective loss of Fe^{2+}, which is accompanied with minor in situ oxidation of Fe^{2+} to Fe^{3+}. Altered basalts from Unit III (Site 801) and Sites 1149 and 765 are also plotted in the diagram in which altered diabases are distinguished from their

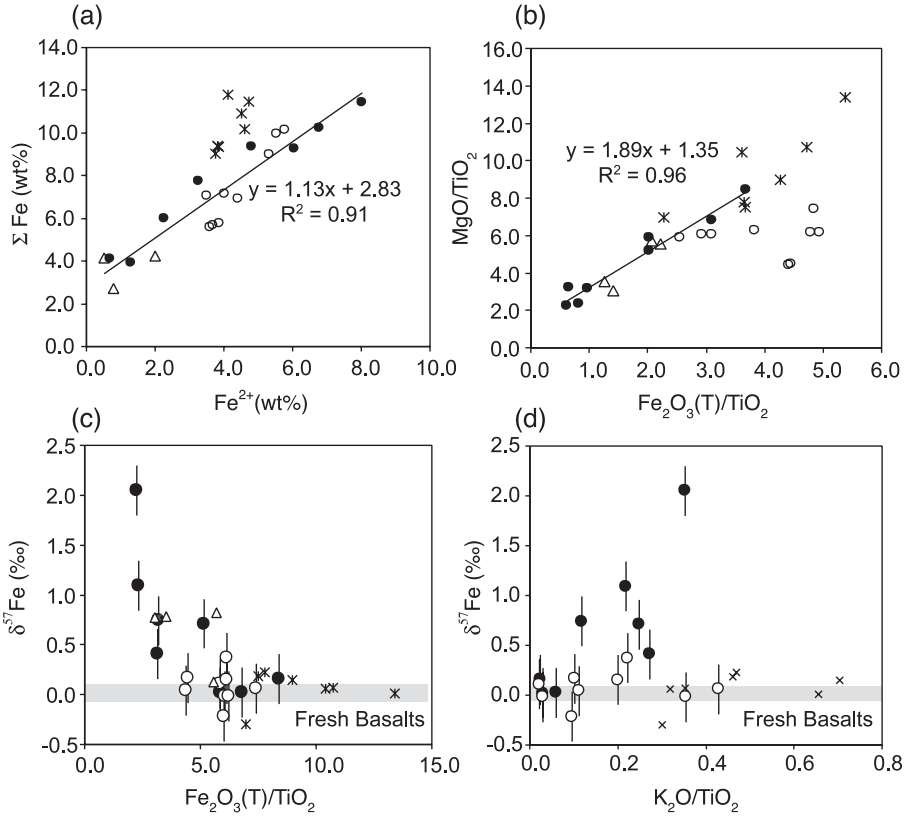

Fig. 6. (a) Correlation between total iron ΣFe and Fe^{2+} of altered pillow basalts underlying Si–Fe hydrothermal deposits in MORB Units I (△) and II (●). Altered basalt at Sites 801 (Unit III) and Sites 1149 and 765 are also plotted (○) together with alteration halos (⁎). The best fit approximation line is $\Sigma Fe = 1.13 \times Fe^{2+} + 2.69$ ($r^2 = 0.89$). The slope in this diagram is close to unity and suggests that the variation of ΣFe in altered basalt is controlled by the selective leaching of Fe^{2+}. (b) Correlation between Mg (MgO) and total Fe (Fe_2O_3) normalized to immobile element Ti (TiO_2) for MORB Units I and II (Site 801C). The combined depletion in Mg and Fe in Units I and II is related to the breakdown of olivine and clinopyroxene, whereas the enrichment in Mg and Fe in alteration halos is due to precipitation of sapontite and Fe-oxyhydroxides. Relationships between δ^{57}Fe values and total Fe content (Fe_2O_3/TiO_2) and K content (K_2O/TiO_2) are presented in plots (c) and (d), respectively. δ^{57}Fe values tend to increase as Fe is depleted. For Fe-depleted samples, δ^{57}Fe values increase follows K enrichment. In contrast, this relationship is not observed for samples that do not undergo Fe depletion.

alteration halos. Alteration halos are enriched in ΣFe relative to adjacent diabase and exhibit an increase in the $Fe^{3+}/\Sigma Fe$ ratio that results from the oxidation and redistribution of Fe from the rock interior toward the rim. This feature is typical of oxidative alteration of seafloor basalt as observed elsewhere (Alt and Honnorez, 1984; Andrews, 1979; Gillis et al., 1992). Petrographical observation of the intensely altered pale green basalts (MORB Units I and II) suggests that more than 80% of primary minerals have been replaced by calcite, smectite (saponite) and celadonite. In addition to losses of Fe, other chemical changes include significant loss of Mg, Mn and gains of K_2O (Fig. 6b).

The δ^{57}Fe values of Fe-depleted basalt associated with the hydrothermal deposits (Units I and II, Site 801) and altered diabase (Sites 801, 1149 and 765) are plotted in Fig. 6c and d as a function of the total Fe content (Fe_2O_3 normalized to immobile element TiO_2) and mobile element potassium (K_2O normalized to TiO_2). Fractionation of Fe isotopes is thus recorded only for Fe-depleted basalts in Units I and II (Fig. 6c), whereas values for average altered basalts (Unit III and diabase with associated halos from Sites 1149 and 765) do not deviate from fresh basalt values. The relationship between δ^{57}Fe values and K_2O (Fig. 6d), which reflect mainly the formation of K-rich secondary clays (celadonite) during seawater–basalt interactions is interesting; for altered rocks from Site 80IC (Unit III) and Sites 1149/765 (including diabase and alteration halos), δ^{57}Fe values do not change with K_2O content which is in marked contrast with samples from Units II and Unit I (not shown in the diagram because K-enrichment is 10-fold higher than for Unit II). Fe-isotope fractionation is thus recorded preferentially in Fe-depleted and K-rich altered basalts, suggesting that high δ^{57}Fe values are probably related to secondary K-rich clays such as celadonite.

Based on the relationship between Fe^{2+} and ΣFe, it is possible to calculate the percentage of Fe^{2+} remaining in the host rocks during alteration. The relationship between the percentage of Fe^{2+} leached during alteration and the δ^{57}Fe values of the Fe remaining in the rocks is presented in Fig. 7 for altered basalts from Site 801 (Units I, II and III) and Sites 1149/765 (diabase). A Rayleigh fractionation model using a solid–liquid fractionation factor

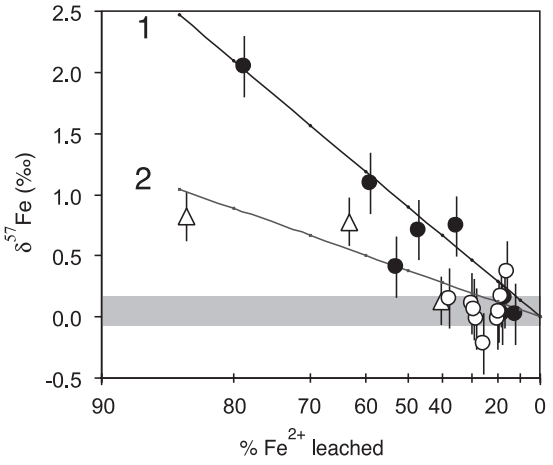

Fig. 7. Values of δ^{57}Fe of altered basalt associated with the Si–Fe hydrothermal in Units I (△) and II (●) versus percentage of Fe^{2+} leached from the rocks. Altered basalts at Sites 801 (Unit III) and Sites 1149 and 765 are also plotted (○). Note log scale on horizontal axis. Fe percentage calculated as $100 \times (Fe^{2+}/\Sigma Fe)sample/(Fe^{2+}/\Sigma Fe)i$ assuming $(Fe^{2+}/\Sigma Fe)i = 0.7$, the ratio of the least depleted sample. Model lines 1 and 2 describe Rayleigh fractionation process for a fractionation factor α of 1.0013 and 1.0005, respectively.

of 1.0005 for the upper (Unit I) and 1.0013 for the lower (Unit II) alteration zones provides an excellent fit to the data. The values for the fractionation factor are greater than 1.0, which indicates that the δ^{57}Fe of the Fe^{2+} released from the host rock, is lower by 0.5–1.3‰ than the initial bulk rock composition.

5. Discussion

Alteration of the oceanic crust occurs through several stages of fracturing, alteration and vein formation (Alt et al., 1986). Therefore, Fe mobilization associated with the alteration processes occurs at different times and under different conditions, which complicates interpretation of the source of Fe-isotope fractionation in the altered oceanic crust. Geochemical cycling of Fe in the oceanic crust is dependant on an intricate interplay between bacterial activity, pH, Eh, temperature, precipitation rate and water/rock ratio. In general, the fate of Fe during oceanic crust alteration involves the alteration of Fe-bearing minerals and the direct precipitation of secondary Fe-bearing minerals from solution. A summary diagram

for the Fe cycling and redox change in the oceanic crust is presented in Fig. 8. We define two major processes:

1. Dissolution–alteration of primary Fe-bearing minerals in basalts and volcanic glass leading to the formation of secondary clay minerals (saponite or celadonite, depending on the condition of alteration, Andrews, 1980) and the release of soluble Fe^{2+} in open cracks. This process may occur abiotically during low-temperature basalt alteration by seawater

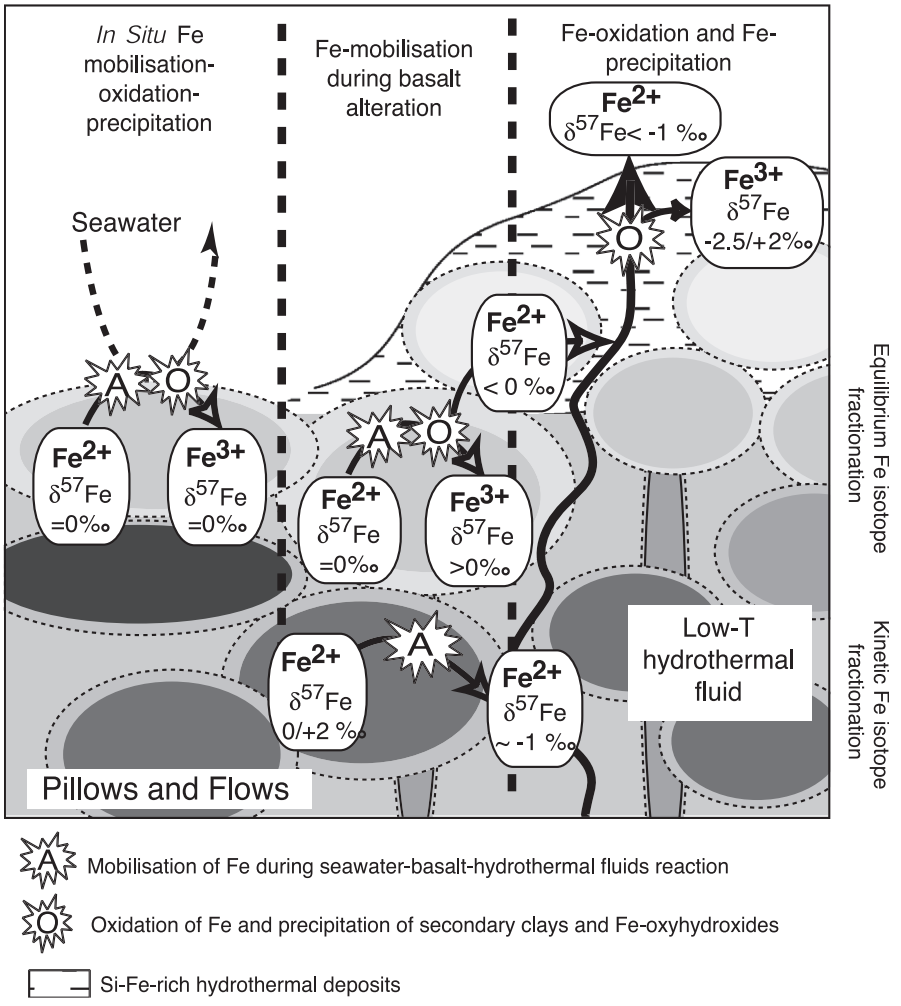

Fig. 8. Summary diagram for the Fe cycling and redox change in the oceanic crust in which three major processes are distinguished: (1) Fe mobilization during seawater–basalt alteration. Fe^{2+} having negative $\delta^{57}Fe$ value relative to the initial rock is released in the low-temperature hydrothermal system. The cause of the light Fe isotope enrichment in leached Fe^{2+} may either be due to kinetic effect during dissolution of primary minerals or due to the formation of isotopically heavy secondary clay during progressive alteration (equilibrium isotope fractionation). (2) Oxidation of Fe^{2+} and Fe precipitation of Fe-bearing secondary clays (celadonite, smectite) or Fe-oxyhydroxides with $\delta^{57}Fe$ values higher than residual Fe^{2+}. (3) A combination of (1) and (2) occurring in situ with no net change in Fe concentration in rocks and consequently with no change in bulk $\delta^{57}Fe$ value. See text for discussion.

(Seyfried and Bischoff, 1979) or eventually through the microbial mediation of Fe-mineral (Liermann et al., 2000) or volcanic glass (Thorseth et al., 2001) dissolution. The Fe-isotope systematics in this process is discussed in Section 5.1.

2. Direct precipitation of Fe-rich phases occurring through oxidation of Fe^{2+}-enriched solutions. This oxidation–precipitation processes is controlled by the mixing of the hydrothermal fluid with seawater. In such environments, Fe is likely to precipitate due to a combination of abiotic and biological processes (Boyd and Scott, 2001). As presented in Fig. 8, in situ mobilization–oxidation–precipitation of Fe is the most common process during seafloor alteration, resulting in the typical alteration halos described in altered basalts (Alt et al., 1986). In this process, oxygen from circulating seawater diffused into the rocks, oxidizing Fe^{2+} from igneous minerals adjacent to the cracks. Fe is thus retained as hydroxides in the halos, whereas it has been lost from adjacent host rocks. The Fe-isotope systematics in this process is discussed in Section 5.2.

5.1. Fe-isotope fractionation during basalt alteration

In this section, we refer to the alteration process associated with leaching of Fe during basalt alteration. Several mechanisms may explain the isotopic fractionation during leaching of Fe from basalts in Units I and II at Site 801C. It is important to underline the fact that these highly leached and isotopically fractionated basalts are found in close association with the hydrothermal deposits (HD I and II in Fig. 5). Alteration reactions possibly took place under sub-oxic conditions, either with seawater at low water/rock ratios or at slightly higher water/rock ratios with evolved seawater that had been depleted in oxygen by previous reactions (Alt et al., 1992). Because the occurrence of Si–Fe-rich hydrothermal deposits is one of the major characteristics of Site 801, the rocks were probably altered through reactions with evolved seawater or low-T hydrothermal fluids that formed and later silicified the hydrothermal deposit. Slightly elevated temperatures (up to about 50 °C) probably increased reaction rates and the extent of alteration (Alt et al., 1992). The chemical changes in MORB Unit I and II include losses of Mg, Fe, Mn and gains of K_2O, suggesting that during interaction between the basalts and the hydrothermal fluids, mobile Fe^{2+} was leached from the host Fe^{2+}-bearing minerals, such as olivine and pyroxene, and a small fraction was reprecipitated in K-rich phases such as celadonite.We note that the range of fractionation factors obtained between dissolved Fe^{2+} and Fe remaining in the rock (1.0005 and 1.0013 in Units I and II, respectively, Fig. 7) is similar to that reported by Brantley et al. (2001) who show that a kinetic effect of up to 1.5‰ in $^{57}Fe/^{54}Fe$ ratio may occur during the ligand-promoted dissolution of Fe at the mineral surface. This is because isotopically light Fe binds to the ligand and is released from the mineral faster than isotopically heavy Fe. In their experimental study, Brantley et al. (2001) observed the largest kinetic effects for biotic experiments using siderophore-producing bacteria, whereas for abiotic experiments without chelates, no isotopic shift was identified. These observations have been interpreted following the kinetic theory, whereby the stronger (biologically produced) ligands should extract lighter Fe. However, isotopic mass balance considerations suggest that a component, which has not yet been identified, with high δ^{57}Fe value, must have been produced in these experiments.

The key to inferring the Fe-isotope fractionation during rock alteration lies in accurate mineral–fluid isotope fractionation factors for secondary clays. Using the calculated reduced partition function ratios for mineral (Polyakov and Mineev, 2000) and hexaquo species (Schauble et al., 2001), we can calculate the δ^{57}Fe values of Fe(II) that might have been in equilibrium with specific minerals, assuming a temperature range of, for example, 25–75 °C. The calculated fractionation factor ($^{57}Fe/^{54}Fe$) between Fe(II) and Fe(II)-rich celadonite is found to be less than 0.5‰, whereas the fractionation factor between Fe(II) and Fe(III)-rich celadonite is in the range of 5–7‰ depending on the temperature. In most cases, the magnitude of predicted fractionations appears to be too great by a factor of 4–10 (Johnson et al., 2003), but these estimations stress the large intrastructural isotope effect between ferric and ferrous ions in celadonite. During low-temperature alteration of basalts under oxic to sub-oxic conditions, various assemblages of secondary clays are formed that include mainly saponite (Fe^{2+}-rich phase) and celadon-

ite (Fe^{3+}-rich phase) (Andrews, 1980). In such processes, the progressive alteration of basalt in an open system would result in the complete dissolution of Fe^{2+}-bearing primary minerals (with no isotopic fractionation). In contrast, in situ partial oxidation of Fe^{2+} and subsequent precipitation of Fe^{3+}-rich celadonite in basalt where residual Fe^{2+} is lost to the fluid would result in isotope fractionation. According to the theoretical calculation considered above, depending on the temperature considered and if isotopic equilibrium is reached, residual Fe^{2+} should be enriched in the light isotope by around 5–7‰ relative to celadonite. Therefore, after complete alteration of the rock, isotopically heavy secondary clays would shift the isotopic composition of the bulk rock to higher values (δ^{57}Fe values of up to 7‰).

The Fe isotopic fractionation of up to 2.05‰ in altered basalts at Site 801C could therefore be consistent with two alternative processes where (1) Fe-isotope signature is the result of kinetic effects stripping isotopically light Fe from minerals, as experimentally observed by Brantley et al. (2001), or (2) the Fe-isotope signature is the result of equilibrium effect between isotopically light Fe(II) leached from the rock and isotopically heavy secondary clays (predominantly celadonite) precipitating in the rock.

In both cases, the Fe-isotope fractionation observed in basalts at Site 801C is related to the extensive leaching of Fe with up to 80% loss of Fe(II) below the hydrothermal deposits probably due to the local high hydrothermal flow. This unique feature may have left a specific geochemical fingerprint in these deposits, which is not observed for other altered basalts at Sites 1149 and 765 for which total Fe in the rocks do not vary significantly. At this stage, it is, however, difficult to differentiate between the major mechanisms (kinetic or equilibrium) of Fe-isotope fractionation under low-temperature hydrothermal conditions. The identification of the fractionation processes requires experimental simulation under controlled laboratory conditions and the determination of specific mineral-pair equilibrium fractionation factors. This issue is of particular importance because the observed δ^{57}Fe variations in altered basalts with preferential leaching of light Fe from the rock are of similar magnitude to those caused by biological alteration (Brantley et al., 2001). Furthermore, low-temperature hydrothermal conditions are highly favorable for the development of a subsurface deep biosphere at the time of alteration, which may have left a specific Fe-isotope signature in these deposits; the identification of such biosignatures are clearly an interesting prospect for future studies in the light of the potential use of isotope biosignatures in ancient and extraterrestrial rocks.

5.2. The variability of Fe isotope composition in secondary Fe-minerals

As shown in Fig. 8, this mechanism refers in particular to Site 801C in which extensive transport and reprecipitation of Fe along fractures (clays and Fe-oxyhydroxides veins) and at the seafloor (Si–Fe hydrothermal deposits) has occurred. In this way, the basaltic section acts as a chromatographic column with respect to Fe-isotope fractionation.

On the basis of field and laboratory studies, Bullen et al. (2001) demonstrated that the mineral ferrihydrite forms as a result of abiotic oxidation of aqueous Fe and contains Fe that is isotopically heavy (~ 1.5‰ for the $^{57}Fe/^{54}Fe$ ratio) relative to coexisting aqueous Fe^{2+}. If secondary Fe-oxyhydroxides are formed within the host rocks, thus increasing the Fe^{3+}/Fe^{2+} ratio, but without significantly changing the total Fe content, the δ^{57}Fe of bulk altered basalt is not expected to change significantly as the system is closed with respect to Fe isotopes. However, we show here that locally Fe^{2+} can be extensively leached from host rock and can have δ^{57}Fe values of -0.5‰ to -1.0‰ lighter than residual altered rock. As the isotopically light fluid flows towards the seafloor, Fe^{2+} in the fluid will first precipitate as secondary pyrite and then oxidize to Fe^{3+} and will later precipitate as Fe-oxyhydroxides through mixing with circulating oxygenated seawater. Therefore, assuming a Rayleigh fractionation process similar to that observed by Bullen et al. (2001), we predict that Fe-oxhydroxides precipitated along the reaction flow path would have δ^{57}Fe values between 0‰ and 0.8‰ at the beginning of precipitation and would become negative during the reaction, producing δ^{57}Fe values as low as -3.0‰ when only 10% of the initial Fe remains in solution. Furthermore, the equilibrium isotopic fractionation between Fe^{2+} and Fe^{3+} in aqueous solutions has been determined to be as

much as 4‰ for the $^{57}Fe/^{54}Fe$ ratio (Johnson et al., 2002). In contrast, rapid oxidation of Fe^{2+} accompanied by rapid precipitation of Fe-oxyhydroxide should produce smaller fractionation, because isotopic fractionation equilibrium is not reached (Johnson et al., 2002). Despite the fact that experimental confirmations are unavailable, Fe-isotope fractionation may also occur during precipitation of secondary clays such as Fe^{3+}-rich celadonite (Polyakov and Mineev, 2000), and as described in Section 5.1, the precipitating phase may be enriched in the heavy isotope by up to 7‰ relative to dissolved Fe(II). Therefore, depending on the degree of isotopic equilibrium of the system, the temperature of reaction, and the type and Fe^{2+}/Fe^{3+} ratio of the precipitated mineral, secondary Fe phases may display a large range of isotopic composition from at least ~ 3‰ down to − 3‰. The large range of $\delta^{57}Fe$ values of secondary sulfides (− 1.07‰ to 0.01‰), clay-rich veins and hyaloclastites (− 2.49‰ to 0.39‰) and Si-rich hydrothermal deposits (− 2.30‰ to 0.58‰) observed at Site 801C strongly favors such reservoir effect, whereby isotope fractionation occurs as Fe^{2+} is released from the basalt and is progressively oxidized and precipitated in open cracks and alteration halos. Hand-picked celadonite-rich vein at Site 801C (sample 801C-43R2, 75/V) yields the highest $\delta^{57}Fe$ values for vein materials (2.05‰), which confirms further that specific mineral fractionation is of major importance in Fe-isotope systematic as has already been suggested by Johnson et al. (2003).

Under the conditions prevailing in the upper oceanic crust, Fe-oxidizing chemolithotrophic microbes can utilize Fe^{2+} as an electron donor for energy generation. Given the very slow rate of oxidation of Fe^{2+} in low-temperature hydrothermal solution and the ubiquitous occurrence of filamentous textures excreted by Fe-oxidizing bacteria in hydrothermal deposits, microbial mediation of Fe precipitation has been invoked as an explanation for the formation of the voluminous Fe oxyhydroxides on the seafloor (Alt, 1988; Boyd and Scott, 2001). These deposits are identical to those recovered at Site 801C, and it is assumed that Fe-oxidizing bacteria are likely to have played an important role on Fe-oxyhydroxide formation within the Fe–Si hydrothermal deposits (Alt et al., 1992). Their effect on Fe-isotope fractionation process remains however unclear as abiotic oxidation process alone is able to produce the range of isotopic composition observed.

5.3. Significance for the geochemical cycle of Fe

An important finding of this study, is that despite the large variation of $\delta^{57}Fe$ values of ~ 4‰ between individual samples in the basement section, the different sections of the oceanic crust are remarkably homogeneous. We suggest therefore that the altered oceanic crust is as a closed system for Fe isotopes (i.e., no isotopic variation at large scale), which is consistent with the observation that despite the fact that basalts display significant Fe mobility during seafloor weathering, the net flux is small (Staudigel et al., 1996).

The most important geochemical change for Fe during seafloor weathering is the oxidation of ferric Fe hosted in primary Fe-minerals to ferrous Fe precipitated as Fe oxhydroxides and Fe-bearing clays. The $Fe^{3+}/\Sigma Fe$ ratio of the altered upper oceanic crust at Sites 801C and 417/418 (Staudigel et al., 1996) is 0.54 and 0.56, respectively, which is around eight times higher than the average ratio (0.07) measured in fresh mid-ocean basalts (Christie et al., 1986). Using an annual weight production rate of 3.606×10^{15} g/year (Staudigel et al., 1996) for the upper 500 m of crust only, we calculate that about 1.3×10^{14} g/year of Fe^{2+} is oxidized to Fe^{3+} during seafloor alteration.

If one assumes that less than 1% of basaltic Fe^{2+} is lost from the upper oceanic crust through diffuse flow at the seafloor (which is within the error of the budget evaluation of Fe during seafloor weathering), 1.4×10^{12} g/year of negative $\delta^{57}Fe$ (presumably below − 1‰) would enter the oceanic system. Despite the fact that the magnitude of this flux is not well constrained, it is significant compared to the high temperature hydrothermal supply of 1×10^{13} g/year or the riverine input of 2.2×10^{13} g/year (Elderfield and Schultz, 1996). Such light Fe from low-temperature oceanic crust alteration would thus be a reasonable candidate for the light Fe component in the high-temperature hydrothermal fluids analyzed recently by Sharma et al. (2001). Of particular importance for the understanding of the budget of Fe isotopes is that leaching of Fe from basalt during hydrothermal pro-

cesses provides the most likely component of ferromanganese crust that have negative δ^{57}Fe values (Zhu et al., 2000b).

6. Conclusions

An important aspect of our results is that both extremely negative δ^{57}Fe values (as much as −2.2‰) and positive δ^{57}Fe values (up to 2.3‰) are found in the oceanic crust basement. Secondary Fe-minerals, such as Fe-oxyhydroxides or Fe-bearing clays have highly variable δ^{57}Fe values that have been interpreted as resulting from the partial oxidation of ferrous iron leached during basalt alteration and precipitation of secondary Fe phases. The variation of Fe-isotope composition of secondary minerals formed during seafloor weathering is thus likely the result of combined effect of mineral–fluid specific isotope fractionation and reservoir effect during mineral precipitation.

Altered basalts at Site 801 C display an increase in δ^{57}Fe values relative to fresh values due to the preferential leaching of light Fe. The apparent fractionation factor between dissolved Fe^{2+} and Fe remaining in the mineral is between 0.5‰ and 1.3‰ and may be consistent with a kinetic effect scenario where Fe-isotope fractionation is the result of chelating ligands stripping Fe from the minerals. However, the formation of secondary clay minerals such as celadonite during basalt alteration may incorporate preferentially the heavy Fe isotopes, resulting in the loss of light Fe isotopes in the fluids. Laboratory experiments are thus required to unravel the processes of Fe-isotope fractionation during basalt alteration and to determine specific mineral–fluid equilibrium fractionation factors.

The Fe-isotope systematics of secondary Fe-bearing minerals (sulfides, Fe-oxyhydroxides and Si–Fe hydrothermal deposits) presented in this study suggests that, despite the fact that Fe oxidation–precipitation processes may be controlled by microbes, such as Fe-oxidizers, the δ^{57}Fe variations of more than 4‰ may be readily explained by abiotic processes alone. At the present state of knowledge, Fe isotopes must be used with caution to determine microbial influences on basalt alteration or to detect life in extreme environments.

Acknowledgements

The authors are grateful to Jean Carignan for analytical facilities and to Katie Kelley for sample preparation and for making available the key samples and analyses of the 801 C composite samples. We thank Albert Galy and Harry Elderfield for providing analytical facilities at Cambridge University to perform Fe isotopes. This study benefited from constructive reviews of Ariel Anbar, Allan Matthews and Clark Johnson. Clark Johnson provided very helpful comments and suggestions. Technical support was provided by the PRISMS-EC grants, contract SMT4 CT 98-2220. **[EO]**

References

Alt, J.C., 1988. Hydrothermal oxide and nontronite deposits on seamounts in the Eastern Pacific. Mar. Geol. 81, 227–239.

Alt, J.C., 1995. Subseafloor processes in mid-ocean ridge hydrothermal systems. In: Humphris, S.E., et al. (Eds.), Seafloor Hydrothermal Systems: Physical, Chemical, Biological, and Geological Interactions. American Geophysical Union, pp. 85–114.

Alt, J.C., Honnorez, J., 1984. Alteration of the upper oceanic crust, DSDP site 417: mineralogy and chemistry. Contrib. Mineral. Petrol. 87, 149–169.

Alt, J.C., Teagle, D.A.H., 1999. The uptake of carbon during alteration of ocean crust. Geochim. Cosmochim. Acta 63, 1527–1535.

Alt, J.C., Honnorez, J., Laverne, C., Emmermann, R., 1986. Hydrothermal alteration of a 1 km section through the upper oceanic crust, deep sea drilling project hole 504B: mineralogy, chemistry, and evolution of seawater–basalt interactions. J. Geophys. Res. 91, 10309–10335.

Alt, J.C., France-Lanord, C., Floyd, P.A., Castillo, P., Galy, A., 1992. Low-temperature hydrothermal alteration of Jurassic ocean crust, Site 801. In: Larson, R.L., Lancelot, Y. (Eds.), Proceedings of the Ocean Drilling Program, Scientific Results. Ocean Drilling Program, College Station, TX, pp. 415–427.

Anbar, A.D., Roe, J.E., Barling, J., Nealson, K.H., 2000. Nonbiological fractionation of iron isotopes. Science 288, 126–128.

Andrews, A.J., 1979. On the effect of low-temperature seawater interaction on the distribution of sulfur in oceanic crust, layer 2. Earth Planet. Sci. Lett. 46, 68–80.

Andrews, A.J., 1980. Saponite and celadonite in layer 2 basalts, DSDP Leg 37. Contrib. Mineral. Petrol. 73, 323–340.

Bach, W., Edwards, K.J., 2003. Iron and sulfide oxidation within the basaltic ocean crust: implications for chemolithoautotrophic microbial biomass production. Geochim. Cosmochim. Acta (in press).

Barr, S.R., Révillon, S., Brewer, T.S., Harvey, P.K., Tarney, J., 2002. Determining the inputs to the Mariana Subduction Factory: using core-log integration to reconstruct basement lithol-

ogy at ODP Hole 801C. Geochem. Geophys. Geosyst. 11, 8901 (doi:10.1029/2001GC000255).

Beard, B.L., Johnson, C.M., 1999. High precision iron isotope measurements of terrestrial and lunar materials. Geochim. Cosmochim. Acta 63, 1653–1660.

Beard, B.L., Johnson, C.M., Cox, L., Sun, H., Nealson, K.H., Aguilar, C., 1999. Iron isotope biosignatures. Science 285, 1889–1892.

Beard, B.L., Johnson, C.M., Skulan, J.L., Nealson, K.H., Cox, L., Sun, H., 2003. Application of Fe isotopes to tracing the geochemical and biological cycling of Fe. Chem. Geol. 95, 87–117.

Belshaw, N.S., Zhu, X.K., Guo, Y., O'Nions, R.K., 2000. High precision measurement of iron isotopes by plasma source mass spectrometry. Int. J. Mass Spectrom. Ion Process. 197, 191–195.

Boyd, T.D., Scott, S.D., 2001. Microbial and hydrothermal aspects of ferric oxyhydroxides and ferrosic hydroxides: the example of Franklin Seamount, Western Woodlark Basin, Papua New Guinea. Geochem. Trans. 7 (doi:10.1039/b105277m).

Brantley, S.L., Liermann, L., Bullen, T.D., 2001. Fractionation of Fe isotopes by soil microbes and organic acids. Geology 29, 535–538.

Bullen, T.D., White, A.F., Childs, C.W., Vivit, D.V., Schulz, M.S., 2001. Demonstration of significant abiotic iron isotope fractionation in nature. Geology 29, 699–702.

Christie, D.M., Carmichael, I.S.E., Langmuir, C.H., 1986. Oxidation states of mid-ocean ridge basalt glasses. Earth Planet. Sci. Lett. 79, 397–411.

Douglas, D.J., French, J.B., 1992. Collisional focusing effects in radio frequency quadripoles. J. Am. Soc. Mass Spectrom. 3, 398–408.

Elderfield, H., Schultz, A., 1996. Mid-ocean ridge hydrothermal fluxes and the chemical composition of the ocean. Annu. Rev. Earth Planet. Sci. 24, 191–224.

Fisk, M., 1999. New shipboard laboratory may answer questions about deep biosphere. EOS 80, 580.

Fisk, M.R., Giovannoni, S.J., Thorseth, I.H., 1998. Alteration of oceanic volcanic glass: textural evidence of microbial activity. Science 281, 978–980.

Furnes, H., Muehlenbachs, K., Torsvik, T., Thorseth, I.H., Tumyr, O., 2001a. Microbial fractionation of carbon isotopes in altered basaltic glass from the Atlantic Ocean, Lau Basin and Costa Rica Rift. Chem. Geol. 173, 313–330.

Furnes, H., Staudigel, H., Thorseth, I.H., Torsvik, T., Muehlenbachs, K., Tumyr, O., 2001b. Bioalteration of basaltic glass in the oceanic crust. Geochem. Geophys. Geosyst. 2 (2000GC000150).

Gillis, K.M., Ludden, J.N., Plank, T., Hoy, L.D., 1992. Low-temperature alteration and subsequent reheating of shallow oceanic crust at Hole765D, Argo Abyssal Plain. In: Gradstein, F.M., Ludden, J.N. (Eds.), Proceedings of the Ocean Drilling Program, Scientific Results, vol. 123. Ocean Drilling Program, College Station, TX, pp. 191–199.

Govindaraju, K., 1994. 1994 compilation of working values and sample description for 383 geostandards. Geostand. Newsl. 18, 1–158.

Govindaraju, K., Mevelle, G., 1987. Fully automated dissolution and separation methods for inductively coupled plasma-atomic emission spectrometry rock analysis. Application to the determination of rare earth elements. J. Anal. At. Spectrom. 2, 615–621.

Gradstein, F.M., Ludden, J.N., 1990. Site 765. In: Gradstein, F.M., Ludden, J.N. (Eds.), Proceedings of the Ocean Drilling Program, Initial Results, vol. 123. Ocean Drilling Program, College Station, TX, pp. 63–267.

Honnorez, J., 1981. The aging of the oceanic crust at low temperature. In: Emiliani, C. (Ed.), Oceanic Lithosphere. Wiley, pp. 525–587.

Johnson, C.M., Skulan, J.L., Beard, B.L., Sun, H., Nealson, K.H., Braterman, P.S., 2002. Isotopic fractionation between Fe(III) and Fe(II) in aqueous solutions. Earth Planet. Sci. Lett. 195, 141–153.

Johnson, C.M., Beard, B.L., Beukes, N.J., Klein, C., O'Leary, J.M., 2003. Ancient geochemical cycling in the Earth as inferred from Fe isotope studies of banded iron formations from the Transvaal Craton. Contrib. Mineral. Petrol. 144, 523–547.

Juniper, S.K., Jonasson, I.R., Tunnicliffe, V., Southward, A.J., 1992. Influence of a tube-building polychaete on hydrothermal chimney mineralization. Geology 20, 895–898.

Larson, R.L., Lancelot, Y., 1992. Proceedings of the Ocean Drilling Program, Scientific Results, vol. 129. Ocean Drilling Program, College Station, TX. 745 pp.

Liermann, L.J., Kalinowski, B.E., Brantley, S.L., Ferry, J.G., 2000. Role of bacterial siderophores in dissolution of hornblende. Geochim. Cosmochim. Acta 64, 587–602.

Matthews, A., Zhu, X.K., O'Nions, K., 2001. Kinetic iron stable isotope fractionation between iron (-II) and (-III) complexes in solution. Earth Planet. Sci. Lett. 192, 81–92.

Plank, T., Ludden, J.N., Escutia, C., et al., 2000. Proceedings of the ODP, Initial Reports, 185 [CD-ROM]. Available from: Ocean Drilling Program, Texas A&M University, College Station, TX 77845-9547, USA.

Polyakov, V.B., Mineev, S.D., 2000. The use of Mössbauer spectroscopy in stable isotope geochemistry. Geochim. Cosmochim. Acta 64, 849–865.

Rouxel, O., Ludden, J.N., Carignan, J., Marin, L., Fouquet, Y., 2002. Natural variations of Se isotopic composition determined by hydride generation multiple collector inductively coupled plasma mass spectrometry. Geochim. Cosmochim. Acta 66, 3191–3199.

Schauble, E.A., Rossman, G.R., Taylor, H.P., 2001. Theoretical estimates of equilibrium Fe-isotope fractionations from vibrational spectroscopy. Geochim. Cosmochim. Acta 65, 2487–2497.

Seyfried, W.E.J., Bischoff, J.L., 1979. Low temperature basalt alteration by seawater: an experimental study at 70 °C and 150 °C. Geochim. Cosmochim. Acta 43, 1937–1947.

Sharma, M., Polizzotto, M., Anbar, A.D., 2001. Iron isotopes in hot springs along the Juan de Fuca Ridge. Earth Planet. Sci. Lett. 194, 39–51.

Staudigel, H., Hart, S.R., 1983. Alteration of basaltic glasses: mechanisms and significance for the oceanic crust–seawater budget. Geochim. Cosmochim. Acta 47, 337–350.

Staudigel, H., Plank, T., White, B., Schmincke, H.-U., 1996. Geochemical fluxes during seafloor alteration of the basaltic upper oceanic crust: DSDP sites 417 and 418. In: Bebout, G., et al.

(Eds.), Subduction: Top to Bottom. American Geophysical Union, Washington, DC, pp. 19–38.

Talbi, E.H., Honnorez, J., 2003. Low-temperature alteration of Mesozoic oceanic crust, ODP Leg 185. Geochem. Geophys. Geosyst. 4, 8906 (doi:10.1029/2002GC000405).

Thorseth, I.H., Torsvik, T., Torsvik, V., Daae, F.L., Pedersen, R.B., 2001. Diversity of life in ocean floor basalt. Earth Planet. Sci. Lett. 194, 31–37.

Torsvik, T., Furnes, H., Muehlenbachs, K., Thorseth, I.H., Tumyr, O., 1998. Evidence for microbial activity at the glass–alteration interface in oceanic basalts. Earth Planet. Sci. Lett. 162, 165–176.

Turner, P.J., et al., 1998. Instrumentation for low- and high-resolution ICP-MS. In: Montaser, A. (Ed.), Inductively Coupled Plasma Mass Spectrometry. Wiley-VCH, New York, pp. 421–501.

Vander Walt, T.N., Strelow, F.W.E., Verheij, R., 1985. The influence of crosslinkage on the distribution coefficients and anion exchange behaviour of some elements in hydrochloric acid. Solv. Extr. Ion Exch. 3, 723–740.

Wheat, C.G., Mottl, M.J., 2000. Composition of pore and spring waters from baby bare: global implications of geochemical fluxes from a ridge flank hydrothermal system. Geochim. Cosmochim. Acta 64, 629–642.

Zhu, X.K., O'Nions, R.K., Guo, Y., Belshaw, N.S., Rickard, D., 2000a. Determination of natural Cu-isotope variation by plasma-source mass spectrometry: implications for use as geochemical tracers. Chem. Geol. 163, 139–149.

Zhu, X.K., O'Nions, R.K., Guo, Y., Reynolds, B.C., 2000b. Secular variation of iron isotopes in North Atlantic deep water. Science 287, 2000–2002.